

**Titre:** Stretchable and Durable Kirigami Inspired Electronics Based on  
Conductive Polymers

**Auteur:** Mina Abbasipour

**Date:** 2022

**Type:** Mémoire ou thèse / Dissertation or Thesis

**Référence:** Abbasipour, M. (2022). Stretchable and Durable Kirigami Inspired Electronics  
Based on Conductive Polymers [Master's thesis, Polytechnique Montréal].  
Citation: PolyPublie. <https://publications.polymtl.ca/10307/>

 **Document en libre accès dans PolyPublie**  
Open Access document in PolyPublie

**URL de PolyPublie:** <https://publications.polymtl.ca/10307/>  
PolyPublie URL:

**Directeurs de  
recherche:** Fabio Cicoira  
Advisors:

**Programme:** Génie chimique  
Program:

**POLYTECHNIQUE MONTRÉAL**

affiliée à l'Université de Montréal

**Stretchable and Durable Kirigami Inspired Electronics Based on Conductive  
Polymers**

**MINA ABBASIPOUR**

Département de génie chimique

Mémoire présenté en vue de l'obtention du diplôme de *Maîtrise ès sciences appliquées*

Génie chimique

Avril 2022

© Mina Abbasipour, 2022.

# **POLYTECHNIQUE MONTRÉAL**

affiliée à l'Université de Montréal

Ce mémoire intitulé :

## **Stretchable and Durable Kirigami Inspired Electronics Based on Conductive Polymers**

présenté par **Mina ABBASIPOUR**

en vue de l'obtention du diplôme de *Maîtrise ès sciences appliquées*

a été dûment accepté par le jury d'examen constitué de :

**Daria Camilla BOFFITO**, présidente

**Fabio CICOIRA**, membre et directeur de recherche

**Noémie-Manuelle DORVAL COURCHESNE**, membre externe

## **DEDICATION**

*This thesis is dedicated to my Family (Maryam, Marjan and Mahin Abbasipour, Michel Bédard, Parmiss and Jalil Fallah), especially my parents (Tayebah Zandieh and Aliasghar Abbasipour) for their unconditional love and support whose encouraged me for tenacity and pushed me for success.*

## ACKNOWLEDGEMENTS

I would like to first express my sincere thanks and appreciation to my supervisor, Prof. Fabio Cicoira, who has always been supportive, helpful and caring ever since I entered the Master program at Polytechnique Montréal. His advice for research has been the constant driving force for my progress and will have a lasting impact on my academic life.

I express my deepest gratitude to my beloved family. I could not come this far without their support and love. They believed in me and taught me that I can overcome any difficulty with patience and hard work.

I am grateful for the funding provided by Institut de l'Energie Trottier through master scholarships and CMC Microsystems for microfabrication grants through programs MNT Financial Assistance and Solutions.

I also would like to thank my friends for their support and friendships as well as my colleagues in the laboratory of iontronics group.

## RÉSUMÉ

L'électronique portable et flexible est une nouvelle technologie qui attire l'attention de nombreux chercheurs en raison de ses applications potentielles dans plusieurs domaines, tels que les capteurs, le stockage d'énergie, les récupérateurs d'énergie et les écrans.

Le principal défi des dispositifs électroniques étirables est de conserver leurs performances électriques et mécaniques sous de fortes contraintes cycliques. La combinaison d'un polymère élastomère et d'un polymère conducteur ainsi que la conception de la structure des dispositifs comptent parmi les stratégies pour fabriquer des structures extensibles et durables. Les dispositifs structurés en kirigami répondent potentiellement à ces critères en raison de leur géométrie unique.

Le kirigami est une ancienne technique de découpage de papier nécessitant des coupes du substrat. Cette méthode a été utilisée pour développer des structures hiérarchiques fonctionnelles pour un large éventail d'applications, tels les capteurs, les échafaudages pour l'ingénierie tissulaire, la conversion d'énergie et les stockages d'énergie.

En ce qui concerne le présent mémoire, le composite polymère constitué du conducteur poly(3,4-éthylène-dioxythiophène): poly(styrène sulfonate) (PEDOT:PSS) et l'élastomère polydimethylsiloxane (PDMS), ainsi que le découpage en kirigami ont été utilisés pour obtenir des dispositifs étirables et fiables. Le découpage au laser a été employé pour fabriquer des échantillons structurés en kirigami.

PEDOT:PSS a été mélangé avec du PDMS (i.e., polymère élastomère) en tant que charge conductrice afin de fabriquer un composite conducteur extensible PEDOT:PSS/PDMS. Dans ce composite, du glycérol et du polyéthylène glycol ont été ajoutés au mélange pour améliorer respectivement la conductivité et l'extensibilité.

Les propriétés mécaniques (i.e., résistance à la traction et viscoélasticité), électriques et électromécaniques du composite polymère PEDOT:PSS/PDMS ont été étudiées.

De plus, les propriétés du composite polymère PEDOT:PSS/PDMS structuré en kirigami ont été comparées aux propriétés du PDMS structuré en kirigami et revêtu de PEDOT:PSS, du PDMS non-structuré en kirigami et revêtu de PEDOT:PSS et du composite polymère non-structuré en kirigami.

Par ailleurs, pour étudier l'effet du revêtement de PEDOT:PSS sur les propriétés mécaniques, des échantillons de PDMS non-structuré et structuré en kirigami, ainsi que revêtus de PEDOT:PSS ont été comparés à des échantillons de PDMS non-structuré et structuré en kirigami, mais sans revêtement.

En outre, l'application du composite polymère à structure en kirigami en tant que capteur de contrainte a été testée pour la détection de mouvements au niveau du poignet. Le capteur a été soumis à l'étirement et à la relaxation cyclique, et la sensibilité et l'hystérésis de résistance électrique ont été étudiées et comparées à l'échantillon de PDMS structuré en kirigami et revêtu de PEDOT:PSS.

## ABSTRACT

Wearable and flexible electronics are new technologies that attract many researchers' attention because of their potential applications in numerous fields such as sensors, energy storage, energy harvesters and displays.

The main challenge of stretchable electronic devices is to maintain their electrical and mechanical performance under high cyclic strain. Mixing an elastomeric polymer with a conductive filler and structural design are among the strategies for fabricating stretchable and durable systems. Kirigami pattern is a kind of structural design that potentially meets these criteria due to its unique geometry.

Kirigami is an ancient papercraft technique created by cuts of a substrate. This method has been used to develop functional hierarchical structures for a wide range of applications such as sensors, tissue engineering, energy conversion and energy storages.

In this thesis, conductive poly (3,4-ethylene-dioxythiophene): poly(styrene sulfonate) (PEDOT:PSS)/ polydimethylsiloxane (PDMS) polymer composite and kirigami patterning were used to make stretchable and reliable conductors. A laser cutting technique was used to fabricate kirigami structured specimens.

PEDOT:PSS as conductive filler was mixed with PDMS (i.e., elastomeric polymer) to make stretchable conductive PEDOT:PSS/PDMS composite. In this composite, glycerol and polyethylene glycol were added to the mixture to improve conductivity and stretchability, respectively.

The mechanical properties (i.e., tensile strength and viscoelastic properties), electrical and electromechanical properties of PEDOT:PSS/ PDMS polymer composite were investigated. In addition, the properties of kirigami structured PEDOT:PSS/PDMS polymer composite were compared to the properties of kirigami structured PEDOT:PSS coated PDMS, non-kirigami structured PEDOT:PSS coated PDMS substrate and non-kirigami structured polymer composite.

To study the effect of PEDOT:PSS coating on the mechanical properties, non-kirigami and kirigami structured PEDOT:PSS coated PDMS were compared to non-kirigami and kirigami structured PDMS specimens.



Furthermore, the application of kirigami structured PEDOT:PSS polymer composite as strain sensor was examined for body movement detection by attaching it to a human wrist. When the sensor was subjected to loading and unloading, the sensitivity and hysteresis of electrical resistance were investigated and compared to the kirigami structured PEDOT:PSS coated PDMS specimen.

## TABLE OF CONTENTS

DEDICATION .....	iii
ACKNOWLEDGEMENTS .....	iv
RÉSUMÉ.....	v
TABLE OF CONTENTS .....	ix
LIST OF TABLES .....	xii
LIST OF FIGURES.....	xiii
LIST OF SYMBOLS AND ABBREVIATIONS.....	xvii
LIST OF APPENDICES .....	xviii
CHAPTER 1 INTRODUCTION.....	1
1.1 Conductive polymers.....	1
1.2 Flexible and stretchable electronic devices .....	2
1.3 Three-dimensional micro/nanofabrication .....	3
1.4 Kirigami pattern .....	3
1.5 Problematics .....	4
1.6 Objectives of thesis .....	5
1.7 Organization of thesis.....	6
CHAPTER 2 LITERATURE REVIEW .....	7
2.1 Stretchable Electrodes .....	7
2.1.1 Embedding conductive fillers in elastomers .....	7
2.1.2 Structural design.....	12
2.2 Application of kirigami structure in electronic devices .....	23
2.2.1 Sensors .....	23
2.2.2 Energy conversion and energy storage devices.....	24

CHAPTER 3	MATERIALS AND METHODS .....	26
3.1	Materials.....	26
3.2	preparation of non-kirigami films .....	27
3.2.1	Fabricating PEDOT: PSS/PDMS polymer composite films .....	27
3.2.2	Fabrication of PEDOT:PSS coated PDMS .....	28
3.3	Preparation of Kirigami structured specimens .....	29
3.4	Scanning electron microscopy (SEM).....	29
3.5	Optical microscopy .....	30
3.6	Mechanical Properties .....	31
3.6.1	Tensile strength .....	31
3.6.2	Viscoelastic behavior .....	31
3.6.3	Behavior in cyclic test.....	32
3.6.4	Dynamic tests .....	33
3.6.5	Electromechanical test.....	33
CHAPTER 4	RESULTS AND DISCUSSION .....	34
4.1	Kirigami pattern .....	34
4.2	Mechanical properties .....	35
4.2.1	Tensile strength .....	35
4.2.2	The behavior of specimens in cyclic tests.....	36
4.2.3	Properties of specimens under dynamic mechanical test .....	40
4.3	Electromechanical properties .....	43
4.4	Application .....	49
CHAPTER 5	CONCLUSION AND RECOMMENDATIONS.....	52
5.1	Recommendations .....	54

REFERENCES..... 55

APPENDICES..... 73

**LIST OF TABLES**

Table 3-1 Chemical structure of used materials.....	27
Table 4-1 Values of $\delta$ , $\tan\delta$ , $E^*$ , $E'$ , and $E''$ for the non-kirigami samples and kirigami structured specimens .....	43

## LIST OF FIGURES

Figure 1.1 Chemical structure of PEDOT:PSS that thiophene monomer attached to ethylene dioxide groups of PSS [3]. .....	1
Figure 2.1 Various methods have been used to fabricate stretchable electrodes [44].....	7
Figure 2.2 Schematic of percolation threshold: arrangement of conductive filler in a polymer matrix (a) disconnected, (b) partially connected, and (c) fully connected [54].....	9
Figure 2.3 (a) making 1D single walled-nanotube (SWCNT) based stretchable conductors, (b) Aligned CNT forest (left), stretching of CNT ribbons (middle) and optical image of folded CNT ribbons applied on PDMS, (c) SEM images of 3D CNT ropes and stress-strain under 20% strain after 1, 10, 100 and 1000 cycles of stretching, (d) a transparent thin film made from SWCNT and PET substrate, and (e) the effect of acid treatment on SWCNT based conducting film [64].....	10
Figure 2.4 (a) methods for fabrication of stretchable conductors [64].....	11
Figure 2.5 Different applications of PEDOT: PSS [72].....	12
Figure 2.6 (a) wavy (upper) and spring-like (lower) structures, (b) making paper stretchable by kirigami cut, (c) improving stretchability using a network straight (left) and serpentine (right) grafts [45]. .....	13
Figure 2.7 The schematic of materials and fabrication methods used for mechanical buckling formation, as well as their applications [78] .....	14
Figure 2.8 Summary of methods for buckling fabrication [78] .....	15
Figure 2.9 In-plane geometries: (a) a serpentine and spiral geometries [79], (b) island-bridge structure [81], (c) horseshoe geometry [82] .....	16
Figure 2.10 A laser cut sheet of paper represents an enlarged image of high stretchable Au nanomesh electrode [77] .....	17
Figure 2.11 Six different patterns of fractal-inspired structure [84] .....	17

Figure 2.12 3D out-of-plane designs: (a), (b) helical structures [85], [88]; (c) and (d) pop-up structures [89], [90].....	18
Figure 2.13 Static origami (a) paper crane and (b) Chinese dragon [94].....	19
Figure 2.14 Different configurations of the magic ball when it exposed to axially or radially force [93] .....	19
Figure 2.15 (a) basic definitions of origami, (b) Miura-ori pattern in folding and stretching states [94], [95].....	20
Figure 2.16 Different patterns of 2D kirigami: (a) with straight cuts [105], (b) a quad kirigami tessellation in closed and open forms [104], and (c) kirigami structures with square and rectangle cuts [35] .....	21
Figure 2.17 3D kirigami structures: (a), (b) 3D kirigami creation from out-of-plane buckling [106], [107], (c) controlling parameters of geometry to make 3D kirigami structure [108], and (d) compression buckled for designing 3D kirigami structure [109].....	22
Figure 2.18 Bistable auxetic kirigami structures [103] .....	23
Figure 3.1 Fabrication of PEDOT:PSS/PDMS polymer composite film.....	28
Figure 3.2 Fabrication of kirigami structured PEDOT:PSS coated PDMS film.....	29
Figure 3.3 Different parts of SEM [136].....	30
Figure 3.4 Different parts of an optical microscope [139].....	30
Figure 3.5 The stress-strain and recovery curves of a material [142] .....	32
Figure 4.1 (a) <i>I</i> : Schematic of kirigami structure in closed form, <i>II</i> : the dimensions of the rotating unit and <i>III</i> : the schematic of one building block in open form; photographs of kirigami structured PEDOT:PSS coated PDMS specimen (b) in closed and (c) open forms; photographs polymer composite specimen in (d) closed and (e) open forms.....	34
Figure 4.2 (a) force-displacement curves of non-kirigami films; (b) force-displacement curves of kirigami structured specimens; (c) Young's modulus and (d) elongation at break of non-kirigami and kirigami structured specimens .....	36

Figure 4.3 Loading/unloading curves under 25%, 35%, 45% and 55% strain for simple (a) non-kirigami) PDMS films, (b) non-kirigami PEDOT:PSS coated PDMS films, (c) non-kirigami polymer composite films, (d) kirigami structured PDMS specimens, (e) kirigami structured PEDOT:PSS coated PDMS specimens, and (f) kirigami structured polymer composite specimens .....	37
Figure 4.4 Loading and unloading curves of (a) simple (non-kirigami) and (b) kirigami structured PDMS, PEDOT:PSS coated PDMS, and polymer composite at 25% strain .....	38
Figure 4.5 50 cycles of loading/unloading under 25% strain at a strain ratio of 1 mm/s and room temperature for (a), (b), (c) non-kirigami and (e), (f), (g) kirigami structured PDMS, PEDOT:PSS coated PDMS and polymer composite, respectively .....	39
Figure 4.6 Energy dissipation for 500 loading/unloading cycles for (a) non-kirigami and (b) kirigami structured samples .....	40
Figure 4.7 Sinusoid curves displacement-time (in blue) and force-time (in red) for non-kirigami (a) PDMS, (b) PEDOT:PSS coated PDMS and (c) polymer composite films versus sinusoid curves displacement-time (in blue) and force-time (in red) for kirigami structured (d) PDMS, (e) PEDOT:PSS coated PDMS, and (f) polymer composite specimens .....	42
Figure 4.8 Current versus time at different applied strains for (a) non-kirigami and kirigami PEDOT:PSS coated PDMS and (b) non-kirigami and kirigami PEDOT:PSS/PDMS composite samples.....	44
Figure 4.9 (a) Optical and (b) SEM images when samples were exposed to 0, 20% and 40% strain. ....	45
Figure 4.10 Current-time graphs of (a) non-kirigami PEDOT:PSS ink coated PDMS fil, and (b) non-kirigami polymer composite film at 25% strain under 1000 stretching/releasing cycles .....	45
Figure 4.11 Current-time graphs for (a) complete period of 5000 opening/closing cycles, (b) initial, (c) 1000, and (d) 5000 opening/closing cycles for kirigami structured PEDOT:PSS ink coated PDMS specimen .....	47



Figure 4.12 (a) photograph and SEM images of kirigami structured PEDOT:PSS coated PDMS specimen after 5000 opening/closing in the open form at the regions of (a) 1, (b) 2, and (c) 3. The scale bar is 100 $\mu\text{m}$ . .....	48
Figure 4.13 Current-time graphs for (a) complete period of 5000 opening/closing cycles, (b) initial, (c) 1000, and (d) 5000 opening/closing cycles for the kirigami structured polymer composite sample.....	49
Figure 4.14 $\Delta R/R_0$ versus strain for (a) non-kirigami and (b) kirigami structured samples at different strains; $\Delta R/R_0$ for opening and closing for (c) kirigami structured PEDOT:PSS coated PDMS and (d) kirigami structured polymer composite samples .....	50
Figure 4.15 (a) Photographs of kirigami structured polymer composite attached to a human wrist, (b) the schematic of electrical circuit used for detecting signals generated by wrist bending, and (c) resistance variation by wrist bending.....	51
Figure A.1 The current-voltage curve of the kirigami sample in closed form (unstrained).....	73
Figure A.2 Calculation of area between hysteresis loop using MATLAB software.....	74
Figure A.3 (a) real image and (b) SEM images of kirigami structured PEDOT:PSS coated PDMS specimen after 5000 opening/closing in the closed-form. The scale bar is 100 $\mu\text{m}$ . .....	75

**LIST OF SYMBOLS AND ABBREVIATIONS**

BaTiO <sub>3</sub>	Barium titanate
CNT	Carbon nanotube
CTAB	Cetyltrimethylammonium bromide
CCD	Charged-coupled device
Cu	Copper
CVD	Chemical vapor deposition
Au	Gold
IPA	Isopropanol
LIBs	Lithium-ion batteries
NWs	Nanowires
TFB	Poly[(9,9-dioctylfluorenyl-2,7-diyl)-co-(4,4'-(N-(4-sec-butyl phenyl)diphenylamine)]
P3HT	Poly(3-hexylthiophene)
PDMS	Polydimethyl siloxane
PSS	Poly(styrene sulfonate)
PVDF	Poly(vinylidene fluoride)
SEM	Scanning electron microscopy
Ag	Silver
SWCNT	Single-walled carbon nanotube
3D	Three dimensional
2D	Two dimensional

## LIST OF APPENDICES

Appendix A	supporting information .....	73
------------	------------------------------	----

## CHAPTER 1 INTRODUCTION

### 1.1 Conductive polymers

Polymers are promising materials for flexible systems because of their intrinsic low mechanical rigidity. In addition, the conductivity and deformability of conjugated polymers make them suitable for developing bendable electronics. Alternating single and double bonds are the basis for obtaining electronic conduction properties in conjugated polymers. Different molecules with this characteristic, such as polyacetylene, polyaniline, polypyrrole, polythiophene, poly(phenyl vinylene) and poly(3,4-ethylene-dioxythiophene) have been studied [1]. Recently, two-dimensional (2D) conductive polymer sheets as well as nonplanar surfaces have been proposed for improving the stability of electronic devices under repeating deformation [2].

Poly (3,4-ethylene-dioxythiophene) (PEDOT): poly(styrene sulfonate) (PSS) has been used by many researchers because of its high conductivity, film-forming, solubility, visible light transmissivity, and stability. PEDOT monomer is a thiophene monomer to which an ethylene dioxide group is attached to carbons 3 and 4 of the aromatic ring. PEDOT shows higher conductivity and thermal stability than other types of conductive polymers. However, the insolubility of PEDOT in most solvents restricts its application. The insolubility problem can be improved by doping PEDOT with water-soluble PSS, which gives PEDOT: PSS [3].

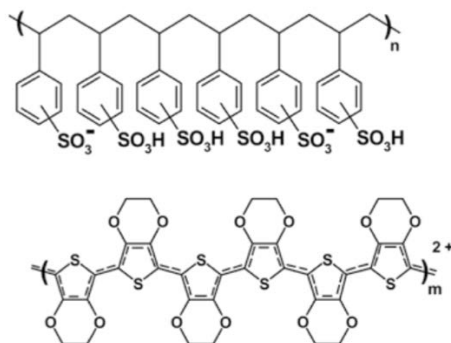


Figure 1.1 Chemical structure of PEDOT:PSS that thiophene monomer attached to ethylene dioxide groups of PSS [3].

## 1.2 Flexible and stretchable electronic devices

Electronic devices with stretchability and bendability can tolerate mechanical deformation and strain while maintaining electronic functionality [4]. This new class of electronic devices is based on a flexible and stretchable substrate. These devices have attracted considerations, especially in biomimetic technologies, because of their mechanical compatibility with the human body [5]. Integrating micro/nanostructure conductive materials with the elastomeric substrate provides new features for obtaining conductivity and stretchability [6]. The main challenge of developing stretchable and flexible electronics is to achieve excellent mechanical deformability and electronic functionality instantaneously. Therefore, the constituent materials in a stretchable system should conserve their mechanical and electrical capability under high strain levels [4].

Wavy design is a method to increase the stretchability of devices. Wavy shapes can be applied for semiconductor nanowires, nanoribbons, and nanomembranes to avoid the fracturing of materials. This method is based on the nonlinear buckling effect, that a thin and rigid layer in a wavy configuration formed on an elastomeric substrate. When the film comprising a thin stiff film and the soft substrate is exposed to mechanical stress, the film removes the surface stress by mechanical buckling. Therefore, the stretchability can be improved by tailoring strain using pre-strain as well as changing the wavelengths and amplitudes of buckles [7], [8].

In another method, stretchable interconnects have been made by blending conductive rigid materials with rubber-like elastomers. This method has been extensively considered because conductive constituents can be integrated into a stretchable substrate by a simple process. Different conductive materials, including metals [9], carbon nanotubes (CNT)s [10], conducting polymers [6] and graphene films have been used for making stretchable interconnects. In addition, various strategies such as vacuum evaporation [11], [12], photolithography [13], and printing [14] have been performed for creating stretchable interconnects on an elastomeric substrate. This process limits to a two-dimensional (2D) structure and has low aspect ratio characteristics, which can be compensated by the substrate [15].

Omnidirectional stretchability in stretchable electronics is a challenge in both methods. Therefore, multidirectional writing of conductive organic and inorganic materials has been performed on elastic substrates in 2D and three-dimensional (3D) designs [16].

### **1.3 Three-dimensional micro/nanofabrication**

Three-dimensional (3D) microfabrication/nanofabrication gives a new dimension to materials with better mechanical, optical, thermal, electrical, acoustic, and magnetic properties than two-dimensional (2D) structures. However, in the past decades, the difficulties and challenges accompanying the 3D fabrication of optical crystals and metamaterials have restricted the research in optical devices. Although 2D materials smooth these issues, the need for developed devices has increased the demand for 3D functionality extension [17].

The micro/nanostructures have extensive applications in electronics/optoelectronics, micro-electro-mechanical systems, medical devices, and cell scaffolds [2]. The top-down (subtractive manufacturing) and bottom-up (additive manufacturing) methodologies have been employed for materials micro/nanofabrication [19]. The top-down strategies are performed in several sequences by masking and removing selective materials [20]. Different types of lithography such as optical lithography, E-beam lithography, soft lithography, nanoimprint lithography, block copolymer lithography, scanning probe lithography, and thermally activated selective topography equilibration are categorized as top-down methods [21]. On the other hand, the bottom-up approach uses physical and chemical phenomena to fabricate nanostructure from simple atoms or molecules [22]. For example, the 3D printing [23], atomic layer deposition [24], sol-gel nanofabrication [25], molecular self-assembly [26], vapor-phase deposition [27], the 2D to 3D transformation by internal forces or external stimuli [28], and mechanical deformation (e. g. curving, folding, rolling, and buckling) [28] are classified as bottom-up methods [21].

### **1.4 Kirigami pattern**

Metamaterials have attracted attention due to their exotic and tunable properties resulting from their unique structural design. Rodger M. Walser defined metamaterials in 1999, which are macroscopic materials with three-dimensional structure and repeating cellular architecture [7]. The

chemical constituents of bulk materials represent their properties. However, the physical properties of metamaterials are dependent on their hierarchical structure [8].

Origami/kirigami structures are metamaterials that suggest structural and properties reconfiguration due to their shape-morphing capabilities [31]. Origami structures have been developed by folding 2D sheets and providing only one degree of axial freedom. Kirigami is a method to make 3D geometries with cuts, and the kirigami structures show additional degrees of freedom. Kirigami is an old Japanese technique in which Kiri means cutting and gami means paper [9]. Kirigami techniques have been used for making functional hierarchical structures in different engineering applications. Kirigami structure contains hinges that can change their geometry by applying force without breaking. Kirigami-inspired metamaterials show unique properties such as negative Poisson's ratio (auxetic metamaterials) [32], multistability [33], coded thermal expansion [34], high stretchability, and compressibility [35]. Materials with kirigami geometry provide high stretchability from rigid materials such as ceramics, metals, and polymers. As a result, mechanical, optical, and electrical properties of materials can be tunable by the kirigami structure [32]. Kirigami structures can be performed on papers, fabrics, polymers, metal sheets, and composites. Laser writing [36], lithography/etching [37], compressive buckling [38], and 3D printing [39] are the main methods used for kirigami pattern creation. The kirigami structures have emerged in a wide range of applications such as space industry, biomedical systems, sensors, optical technologies, energy harvesting, and energy storage.

## 1.5 Problematics

A highly stretchable electrode is a crucial constituent of flexible and wearable devices. Usually, a conducting electrode is made by coating a conducting layer onto an elastomeric substrate such as polydimethylsiloxane (PDMS). When cyclic stretching or other severe circumstances are applied to electrodes, debonding and delamination occur at small strain due to the significant difference between mechanical and surface properties of the metal or carbon conductor and an elastomeric surface [40]. Therefore, poly(3,4-ethylenedioxythiophene): polystyrene- sulfonate (PEDOT: PSS) is a conductive polymer used as a conductive layer.

The main challenge in stretchable electronics is maintaining electrical and mechanical performance (i.e., durability) under high mechanical and cyclic strain. In addition, accommodating multidirectional strain is critical in wearable and stretchable electronics. Most studies have used unidirectional kirigami structures to fabricate extensible conductors [41]–[43]. When uniaxial stretching is applied to the simple structure of PEDOT:PSS coated PDMS, cracks and wrinkles are formed due to strain. These structural damages have a detrimental effect on device durability. Engineering the geometry of the device, such as the kirigami pattern, can improve the stretchability of the device.

On the other hand, the mechanical difference between PDMS (elastic) and PEDOT:PSS (brittle) results in the elasticity mismatch at the interface between them. Thus, polymer composite is a possible way to restrict cracks and wrinkles by strain. Therefore, in this project, kirigami structured PEDOT: PSS/PDMS polymer composite has been suggested to enhance stretchability as well as durability.

## **1.6 Objectives of thesis**

The main objective of this project is to develop stretchable and durable electrodes using kirigami patterns and polymer composites. Applying kirigami structure to composite materials meets structural requirements for wearable devices.

The following specific objectives have been considered to meet the main objectives:

- 1- Fabricating kirigami pattern PDMS by laser cut and coating with PEDOT: PSS by spin-coater for making electrode
- 2- Fabricating PEDOT:PSS polymer composite and then creating kirigami pattern by laser cut
- 3- Investigating mechanical properties of kirigami structured films and non-kirigami films
- 4- Investigating the effect of PEDOT:PSS coating on mechanical properties of PDMS
- 5- Determining electrode stretchability using electromechanical tester machine in different strains such as 30%, 75%, 100%, and 200%.



- 6- Determining the electromechanical stability of samples after 1000 and 5000 cyclic loading/unloading.

## **1.7 Organization of thesis**

The rest of this thesis is organized as follows: This thesis begins with a literature review. Chapter 2 explains different methods for improving stretchability. This chapter also reviews various applications of the kirigami approaches for electronic devices such as sensors, energy harvesters, and energy storage devices. Chapter 3 discusses the experimental part of the thesis, including manufacturing and characterizing kirigami-structured electrodes. Chapter 4 discusses the obtained results and presents a kirigami structured polymer composite application as a strain sensor for human body movement detection. Finally, Chapter 5 concludes this thesis by reviewing its main contributions and potential future work.

## CHAPTER 2 LITERATURE REVIEW

### 2.1 Stretchable Electrodes

Developing of skin-inspired electronics causes intensive requirements of stretchable electrodes. Electrodes are the main component in electronic devices, so the stretchability of electrodes is crucial in flexible and stretchable electronic devices. The main characteristic of stretchable electrodes is the maintenance of their electrical properties under mechanical deformation. Therefore, this kind of electrode should have the capability to bend and deform without the occurrence of damage. Figure 2.1 shows different strategies used in various studies.

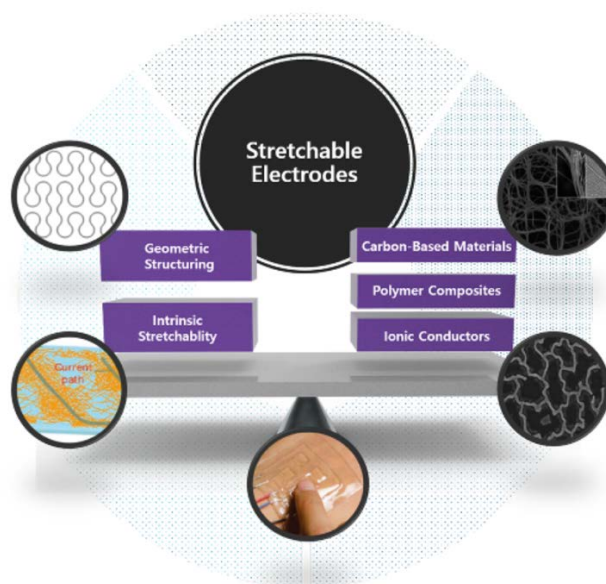


Figure 2.1 Various methods have been used to fabricate stretchable electrodes [44]

#### 2.1.1 Embedding conductive fillers in elastomers

Different nanomaterials such as CNT, graphene sheet, metal nanowires (NWs), conductive polymers, and nanocomposites have been investigated for stretchable electrodes. Graphene with low sheet resistance ( $100\text{-}1000\ \Omega\ \text{sq}^{-1}$ ), high transparency of 90%, and durability for a few cycles

at 6% strain attracted attention for flexible electronics [45]. The stretchability of graphene increased by nanobridge creation through graphene structure.

Ultrathin metal films like silver (Ag), copper (Cu), and gold (Au) showed conductivity with low resistance [45]. The thickness of metal film has an impact on resistance. The thickness should be more than the percolation threshold. However, the resistance of thick film increases under high strain [45]. Under high tensile stress, NWs separate and move against each other, causing high contact resistance. Therefore, NWs cannot return to their initial state when the stress is released. The research in [46] showed that the stretchability of Ag NWs increased 130% by interconnecting Ag NWs with graphene oxide. Combining conductive fillers such as metal nanostructures, CNT, or graphene with elastic polymer is a way to fabricate stretchable electrodes. Various methods such as electrospinning [47], ink-jet printing [48], and spin/blade coating [49] have been used to create a thin layer of conductive material on stretchable substrates like polydimethylsiloxane (PDMS) and polyurethane (PU). For example, Shin et al. [50] constructed a stretchable transistor using Au nanosheet as an electrode and electrospun poly(3-hexylthiophene), P3HT, nanofibers as an active channel. This device showed electrical durability > 1500 stretching cycles.

Ionic conductors are a new class of conducting materials that shows transparency and stretchability. The resistance of ionic conductors is more than metal electrodes without stress. However, their resistance is less than metal electrodes under mechanical deformation [45].

Liquid metals such as mercury and gallium are another class for conducting metal electrodes that offer unlimited deformability. Therefore, this type of conducting materials has been suggested for flexible and stretchable electronic devices. In addition, this material showed low resistance ( $2.95 \Omega \text{ sq}^{-1}$ ) under strain > 100%. On the other hand, liquid metals have important disadvantages such as low chemical stability, unstable contacts between liquid metals and other metal connectors, and difficulty in controlling the movement of liquid metals.

In addition, blending a conductive filler into a soft elastic material has been offered for producing rubber-like electrodes. The conductive filler within polymer media produces a network for electrical interconnectivity [51]. This interconnect electrical conductivity is determined by the percolation theory [52]. The percolation theory expresses the minimum amount of conducting filler

needed for changing an insulating polymer to a conducting polymer. This amount is called the percolation threshold [52]. Therefore, electrical current moves through the conductive fillers network (Figure 2-1). For example, Lee et al. [53] embedded Ag NWs into elastic (ECOFLEX) substrate. This combination maintained its electrical performance at strain > 460%. Reducing electrical conductivity with strain is the main problem of this method [44].

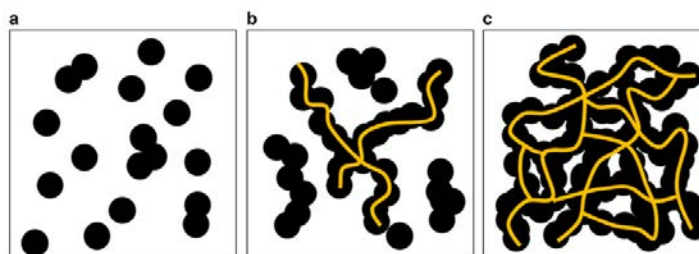


Figure 2.2 Schematic of percolation threshold: arrangement of conductive filler in a polymer matrix (a) disconnected, (b) partially connected, and (c) fully connected [54].

Another example of blending conductive filler with elastomeric material is the work done by Sekitani et al. [55]. A highly stretchable conductive film was fabricated by blending Single-walled carbon nanotube (SWCNT)/ionic liquid mixture into a fluorinated copolymer. This composite film showed  $57 \text{ S cm}^{-1}$  at the unstretched position and maintained its conductivity at 38% strain. However, conductivity changed to  $6 \text{ S cm}^{-1}$  when 134% strain was applied. The SWCNT polymer composite film showed good reliability under different stretching cycles. For example, conductivity mainly remained constant after 4000 cycles, 500 cycles for 25% and 50% stretching, respectively (Figure 2-2a) [55].

To have better stretchability, CNT with different configurations has been developed. The highly aligned CNT ribbon embedded in the PDMS substrate could maintain its conductivity under 100% strain (Figure 2-2b) [56]. The CNT ribbon aligned along its axial direction could maintain its contact under stretching. Moreover, the CNT ribbon was transparent and lightweight. The stretchability of CNT improved by changing its configuration to yarn [57], [58]. Van der Waals interactions hold aligned CNT arrays together, so mechanical strength improved [58]. Shang et al. [59] made spring-like CNT rope to enhance tensile strength to 285%. The resistance changes were about 2% after 1000 stretching/releasing cycles at 20% (Figure 2-2c) [59]. Figure 2e shows a thin,

transparent SWCNT film applicable to optoelectronics, solar cells, and transistors [60]. Lipomi et al. [61] made a skin-like pressure sensor using transparent ( $> 88\%$ ) and conductive ( $2200 \text{ S cm}^{-1}$ ) CNT films. This film could sustain its conductivity at 150% strain. Although CNTs have many advantages, improving their conductivity is important. Their electrical conductivity can be improved by chemical doping or functional group modification [62], [63]. For example, Nitric acid treatment could enhance the conductivity of CNT by 2.5 times [62].

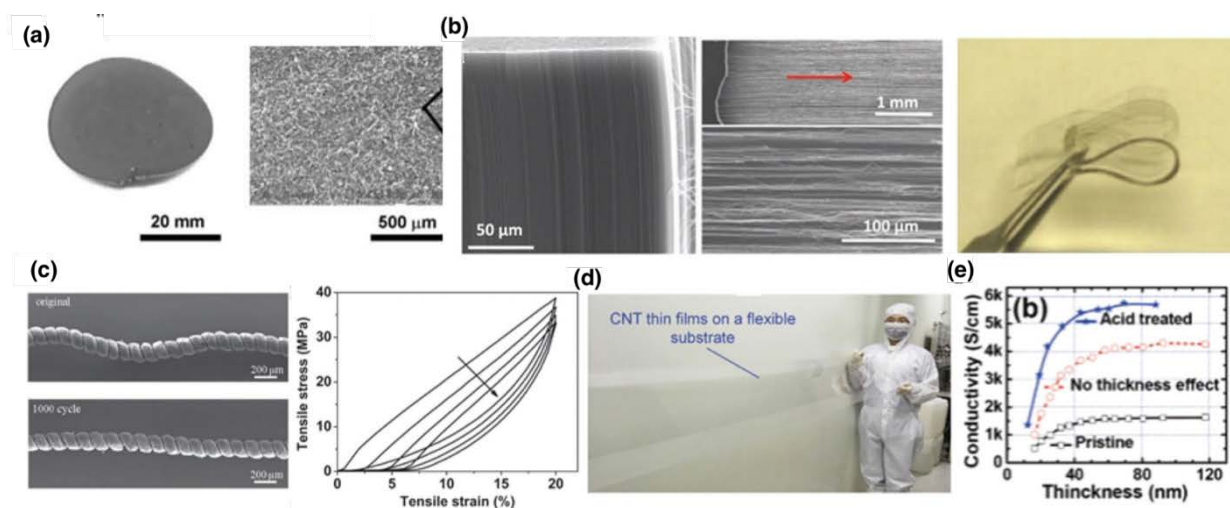


Figure 2.3 (a) making 1D single walled-nanotube (SWCNT) based stretchable conductors, (b) Aligned CNT forest (left), stretching of CNT ribbons (middle) and optical image of folded CNT ribbons applied on PDMS, (c) SEM images of 3D CNT ropes and stress-strain under 20% strain after 1, 10, 100 and 1000 cycles of stretching, (d) a transparent thin film made from SWCNT and PET substrate, and (e) the effect of acid treatment on SWCNT based conducting film [64].

Different strategies are considered for making stretchable conductive materials (Figure 2-3). High quality films can be fabricated by direct chemical vapor deposition (CVD) and array drawing approaches. These methods are more expensive than the wet process. However, it is difficult to reach high quality film in the wet process. Solution-based methods such as mixing, drop-casting, and spin-coating are low-temperature processes. These methods have the ability for large-scale production and can be used in different substrates [64]. So, solution-based methods are favored in industrial applications because these methods reduce the problem of choosing the type of materials and substrate size compared to the conventional process for semiconductor manufacturing.

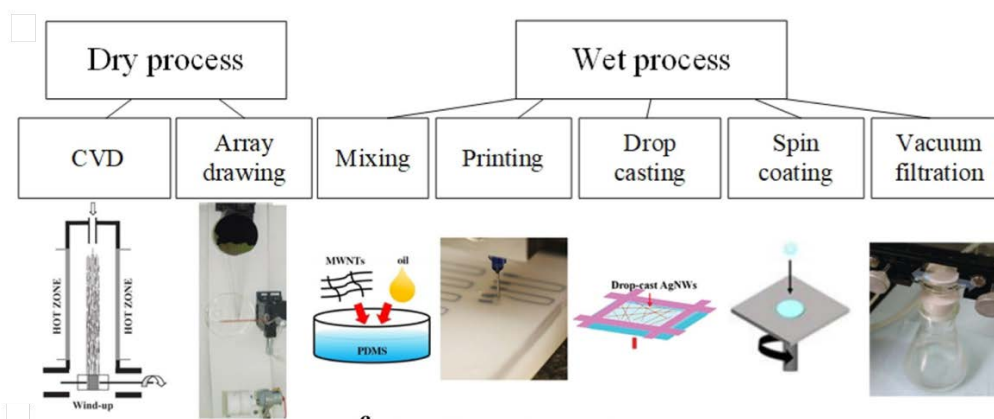


Figure 2.4 (a) methods for fabrication of stretchable conductors [64].

The type of fillers and elastomers and fabrication process impact the electrical and mechanical properties of the conductors [64].

Conducting polymers are lightweight and flexible, so they are desirable for electronic devices applications. In addition, they have unique properties such as thermal stability, high transparency in the visible region, and high conductivity leading to many studies on PEDOT: PSS for organic electronic applications [65]. For example, Wang et al. [66] fabricated a PEDOT: PSS composite film, which showed high conductivity ( $3600 \text{ S cm}^{-1}$ ) after 1000 cycles under 100% strain. The conductivity was  $100 \text{ S cm}^{-1}$  at 600% strain. Furthermore, incorporating plasticizers such as fluorosurfactants not only increased conductivity but also enhanced stretchability [67]. PEDOT: PSS is a conductive and transparent polymer that has been used in various organic electronics such as polymer light-emitting diode [68], organic solar cells [69], transistors [70], and supercapacitors [71] (Figure 2-5).

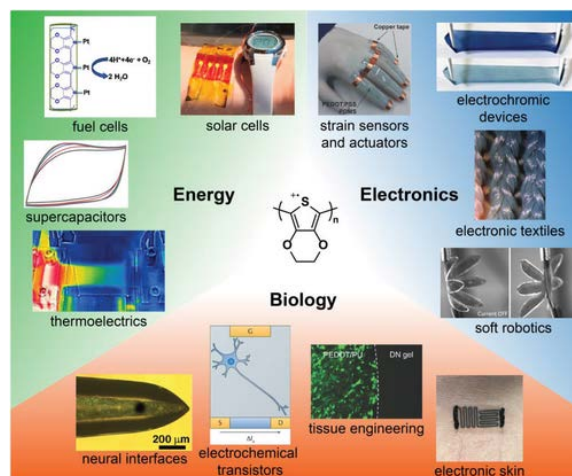


Figure 2.5 Different applications of PEDOT: PSS [72]

### 2.1.2 Structural design

Typically, inherent stiff conductive materials such as metals have no stretchability. However, applying sufficient structural geometries makes them stretchable. The mechanical buckling method is a way to provide a wavy structure on an elastic substrate [73]. Different types of structural designs such as wavy [74], serpentine [75], and spring-like [76] have been suggested for converting brittle inorganic conductive materials to stretchable ones by applying strain (Figure 2.6a) [8]. Spring-like or ribbon shape of CNT film increased tensile strength by over 100% [40], [56]. Usually, the electrodes with nanomesh structure are more stretchable than the percolation network in the strain state. Figure 2.6b shows that an engineered geometry on paper can convert the paper from rigid to elastic. Maintaining conductivity at high stretching can be adjusted by in-plane motions like changing amplitudes and wavelengths of the waves [8]. The serpentine model of metals made them ideal for stretchable electrodes. However, fabricating a nanoscale network of serpentine from metal is technically difficult. The grain-boundary lithography was used to fabricate 2D Au with serpentine geometry on PDMS. The Au nanomesh on PDMS had 160% stretchability, while resistance increased from 21 to 65  $\Omega \text{ sq}^{-1}$ . In addition to serpentine structure, an in-plane sinusoidal wavy structure caused high mechanical deformability. For example, the buckled Au network was stable at 100% strain for 100000 cycles [77]. Maintaining conductivity at the high strain in nanomesh structure can be accommodated by in-plane and out-of-plane movements [77].

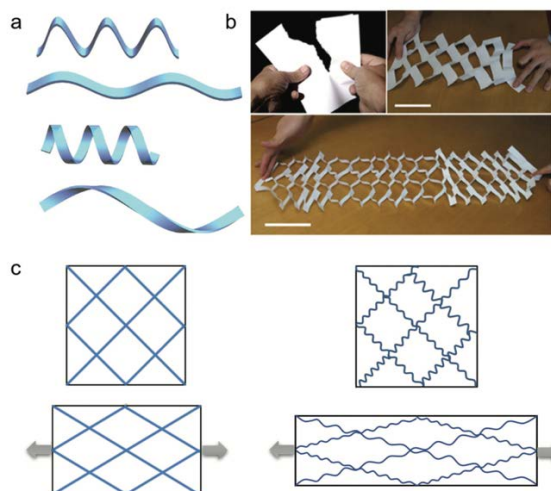


Figure 2.6 (a) wavy (upper) and spring-like (lower) structures, (b) making paper stretchable by kirigami cut, (c) improving stretchability using a network straight (left) and serpentine (right) grafts [45].

### 2.1.2.1 Structural design by buckling phenomenon

The buckling phenomenon has been used to fabricate wavy structures on elastomeric surfaces. Inherent rigid materials convert to stretchable ones by buckling [4]. A rigid conductive material is attached to a pre-strained elastic surface to make it wrinkled when it is released (Figure 2-7) [64]. The wavy patterns can be grown unidirectionally, multidirectional, or hierarchically. Figure 2-7 shows a schematic of materials and fabrication methods used for mechanical buckling formation, as well as their applications [78].



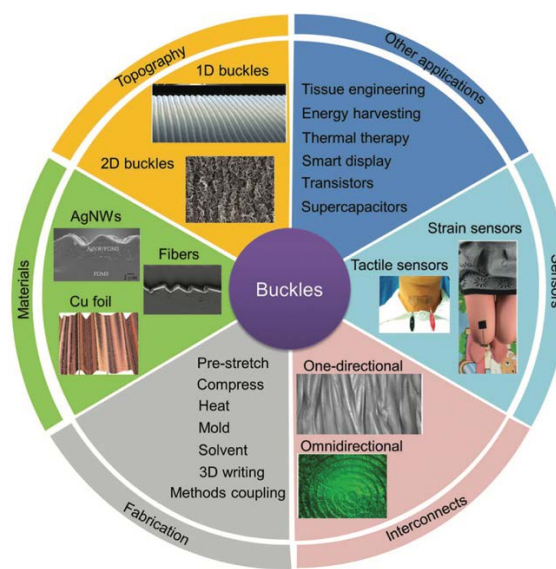


Figure 2.7 The schematic of materials and fabrication methods used for mechanical buckling formation, as well as their applications [78]

Several mechanisms such as stretching/releasing, mechanical compression, solvent and heat deformation, and substrate molding have been used for buckling formation (Figure 2.8) [78]. The most common method is the stretch/release method. In this method, a conductive layer is deposited to a pre-strained substrate. When the stretch releases, out-of-plane or in-plane buckle forms due to mechanical mismatching of two layers. In this method, a pre-strain ratio can control the wavy structure [44]. In the compression method, when the strain is released in the pre-strain substrate, compressive stress is generated, which causes buckle formation [78].

Solvent-induced buckles come from an osmotic force by swelling ratio differences between several components. For example, a soaked paper in the water shows a wrinkled pattern after drying. It is possible to make a uniform pattern on a sponge-like substrate from this method [78]. In the thermal method, a conductive layer is deposited on a high-tempered substrate, and wrinkles form during the cooling process due to compressive force [78].

Using a pre-patterned substrate is another method to fabricate wavy structures by buckling formation. The pre-patterned substrate is prepared via different methods such as lithography, chemical etching, 3D printing, and bio-inspired templating [78].

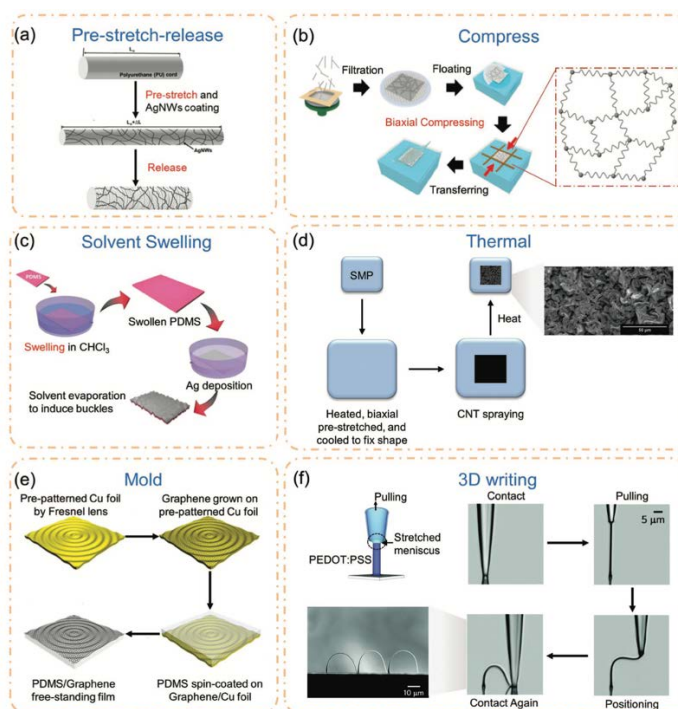


Figure 2.8 Summary of methods for buckling fabrication [78]

The buckling mechanism can be applied on two classes of conductive materials, including: I) 2D continuous thin films obtained from chemical vapor deposition, spin-coating conductive polymer, and assembly of 0D nanoparticles II) 1D nanowires (NWs) such as Ag NWs, Cu NWs, metal oxide nanowire and conductive polymer nanofibers [78].

In the buckling method, cracks and delamination happen due to weak interfacial adhesion between the conductive layer and the substrate. The type and thickness of conductive materials as well as the adhesive between support and conductive layers affect the interfacial adhesion [78]. Good adhesion of conductive materials and substrate is achieved by methods like plasma and surfactant treatment [44].

### 2.1.2.2 2D in-plane design

The 2D in-plane design is constructed by repeatable microstructures that every single element gives stretchability to the whole structure. Different patterns such as 2D polygonous, serpentine, hierarchical triangular, diamond, hexagon, and horseshoe are categorized into this group.

The type and thickness of conductive materials, line width, lattice geometry, and aspect ratio affect the mechanical performance of the whole structure. Island-bridge and mesh network designs, which have more stretchability than single serpentine design, are developed to improve mechanical performance. In this structure, rigid materials are used as islands, and metal interconnects with in-plane or out-of-plane geometry are used as bridges. The disadvantage of the interconnects with out-of-plane geometry is the difficulty of fabricating them with rapid and simple ways such as roll-to-roll and printing. In-plane structures like zigzag, horseshoe, and spiral have been suggested to make interconnects for island-bridge structures. The spiral geometry proposed better stretchability than serpentine under 325% strain without rupture [79], [80].

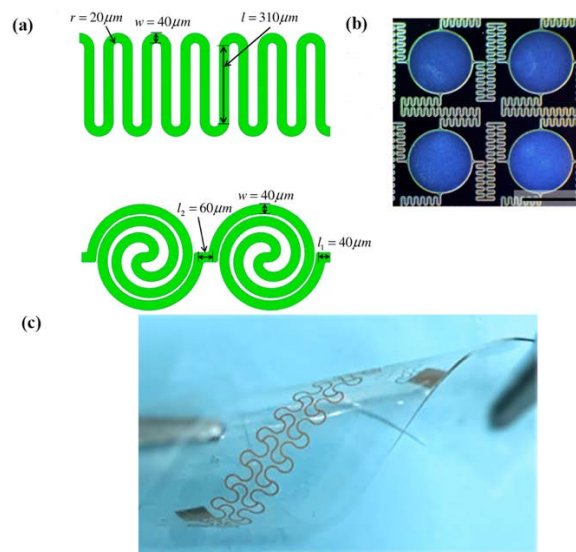


Figure 2.9 In-plane geometries: (a) a serpentine and spiral geometries [79], (b) island-bridge structure [81], (c) horseshoe geometry [82]

Another geometry in the 2D in-plane group is the metal nanomesh network (Figure 2.10). Metal nanomesh network suggests a more deformable structure than metal nanowires. The conductivity of the nanomesh network reduces significantly under strain lower than 100%. Nanomesh network can accommodate strain in two different manners [83]:

- I) When a small strain is applied to the structure, the in-plane movement happens by which the length increases, and the width becomes narrow

II) At high strain, the nanomesh network shows out-of-plane deformation [83]

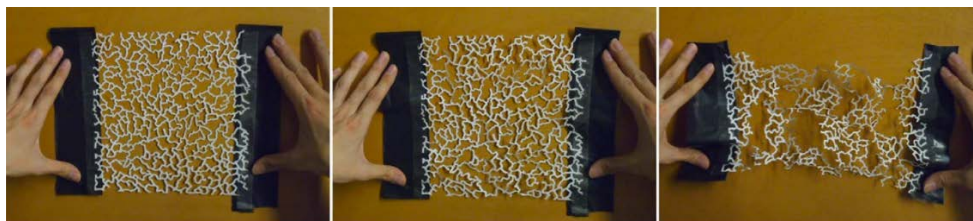


Figure 2.10 A laser cut sheet of paper represents an enlarged image of high stretchable Au nanomesh electrode [77]

Another class of these engineered geometries is fractal topologies which are fabricated using lines and loops. Figure 2.11 shows an example of a fractal-based structure. Among all fractal designs, horseshoe fractal has better stretchability. The optimum stretchability of the horseshoe fractal can be obtained by changing the arc angle to 235 degrees. Therefore, the high-order fractal horseshoe has a lower elastic modulus than the usual horseshoe pattern [64].

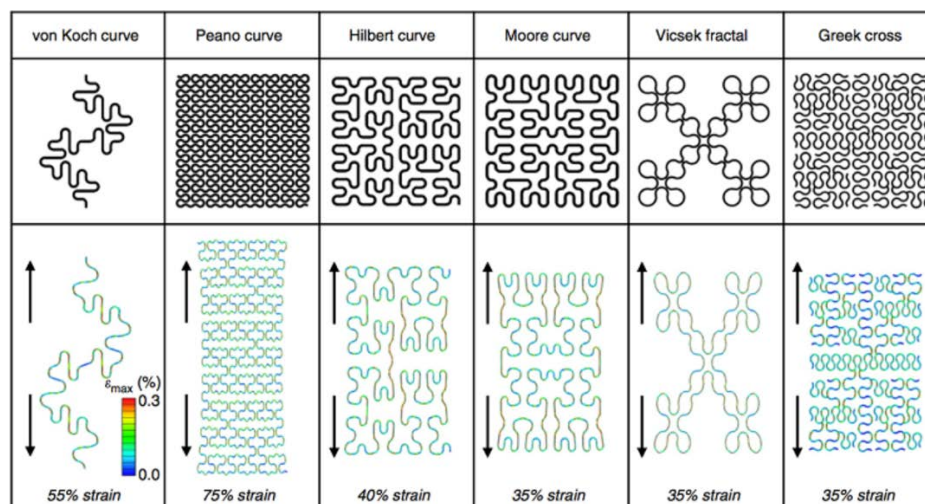


Figure 2.11 Six different patterns of fractal-inspired structure [84]

### 2.1.2.3 3D out-of-plane design

The helical structure is the most common 3D out-of-plane design. This configuration has better mechanical performance than 2D designs. However, the interfacial connection between conductive

materials and support substrate is an important issue. The helical structured electronic device had stretchability up to 600% and could maintain its electrical performance under 1000 stretching/releasing cycles at 100% strain [85]–[87]. Figure 2.12a shows the photograph and SEM images of helical geometry.

The pop-up structure is another out-of-plane design that improves the stretchability of wavy or wrinkled structures 5-10 times. The pop-up structure is comprised of two parts, island and bridge. The bridge parts have wavy or wrinkled structures, which connect to the substrate (island) at nodes. When mechanical strain is applied to the pop-up structure, the wrinkled structures open, and the interconnects become straight [86]. Figure 2.12b shows the pop-up structures.

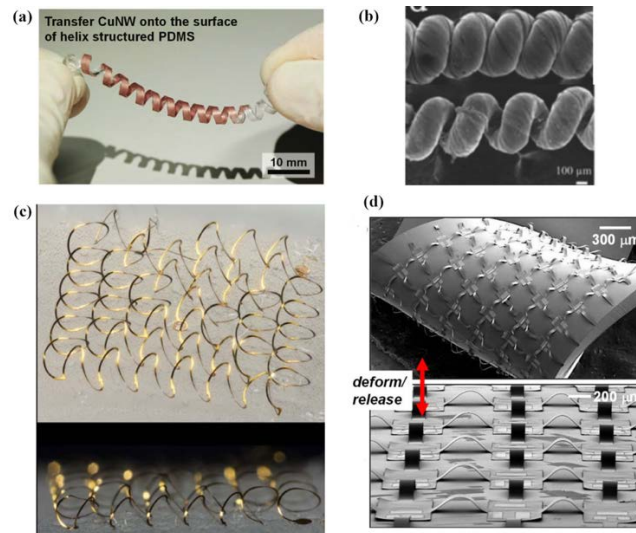


Figure 2.12 3D out-of-plane designs: (a), (b) helical structures [85], [88]; (c) and (d) pop-up structures [89], [90]

Other out-of-plane configurations were inspired by nature. For example, elastomeric petals were inspired by rose petals. The elastomeric petals were obtained from a PDMS surface, and then a thin layer of Cu film was electrodeposited [91]. This kind of structure had unidirectional stretchability to 90%, and it was durable for 1000 stretching/releasing cycles under 40% strain [91]. In addition, Mogul-patterned structure arranged in hexagonal closed packed structure shows multidirectional stretchability [92].

### 2.1.2.4 Origami

The ancient papercraft techniques such as origami and kirigami are ways to create 3D structures. The idea of engineering geometry in paper art was first offered by Miura [93]. Figure 2.13 shows the simple origami paper crane and Chinese dragon as static origami.

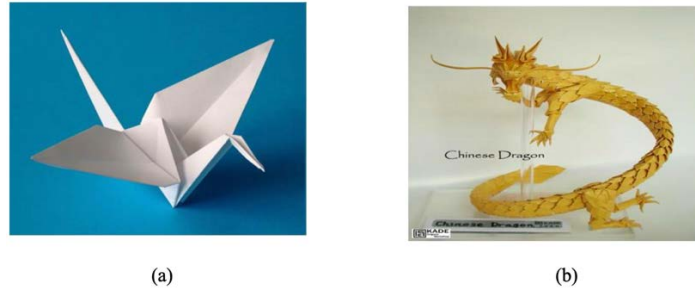


Figure 2.13 Static origami (a) paper crane and (b) Chinese dragon [93]

Rigid origami is a kind of origami that can be deformed at creases. However, the facets between the creases are not subjected to deformation. Miura-ori pattern, waterbomb base, Yoshimura pattern, and diagonal pattern are all common shapes of rigid origami patterns [94]. “Water bomb” or “magic ball” can be deformed spherically or cylindrically when the applied force is axially or radially, respectively [93].

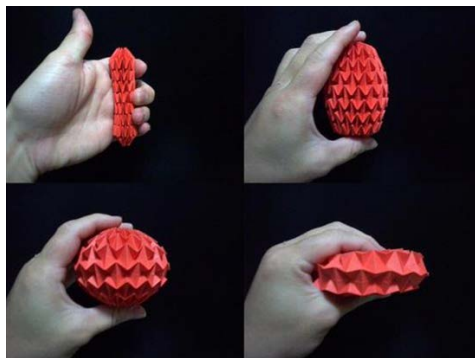


Figure 2.14 Different configurations of the magic ball when it exposed to axially or radially force [93]

In origami pattern, the creases indicate the created lines when the paper is bent. The creases are divided into mountain and valley creases according to their direction. The intersection points of the creases are called vertices. The areas between creases are facets of origami (Figure 2.15a) [94]. Another well-known pattern of origami is Miura-ori pattern which has one-degree-of freedom. By applying force through the Muira-ori pattern, the diagonal line can be transferred to an unfolded state (Figure 2.15b) [95].

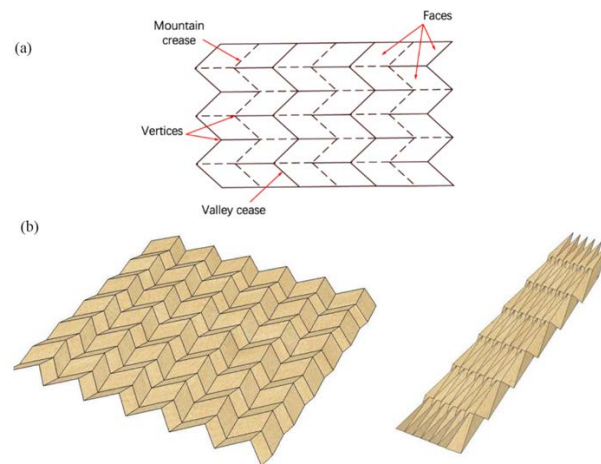


Figure 2.15 (a) basic definitions of origami, (b) Miura-ori pattern in folding and stretching states [94], [95]

Different origami forms can be created from the folding method obtained by six Huzita Axioms and one Hatori Axiom [96]. In addition to electronic devices, origami pattern has been explored for biomedical applications such as cardiac catheterization [97], drug delivery [98], microgrippers [99], and microfluidic devices [100].

Although it is possible to design different patterns by folding in origami geometries, the planar facets still limit the deformability of origami structures. Also, their deformability is limited because they can just transfer from fold state to planar state [95].

### 2.1.2.5 Kirigami

Kirigami patterns have been suggested to improve sheets' deformability [101]. Kirigami is a pattern created by cuts or the combination of cuts and folds. The pattern for kirigami cuts can be originated

from the tiling of old architectures [102], [103]. A simple kirigami pattern contains straight lines at constant distances. In [104], when a strain was applied on a simple kirigami structure, the edges of the pattern showed out-of-plane deformation (Figure 2.16a). Three kinds of deformation occur in correspond to an applied stress: 1) under small stretching, the in-plane deformation happens, 2) by increasing the strain, out-of-plane deformation is created at the edges, 3) at the end, the gap between cuts becomes narrow until structure breaks [104]. Another 2D structured kirigami pattern design is kirigami with quad tessellation formed by flat cutting (Figure 2.16b) [105]. The cuts in the edges provide in-plane rotational of hinges in open form. Tang et al. [35] investigated the effect of cuts geometry on stretchability (Figure 2.16c). They concluded that stretchability increased from 41% for square units to 124% for a rectangle shape.

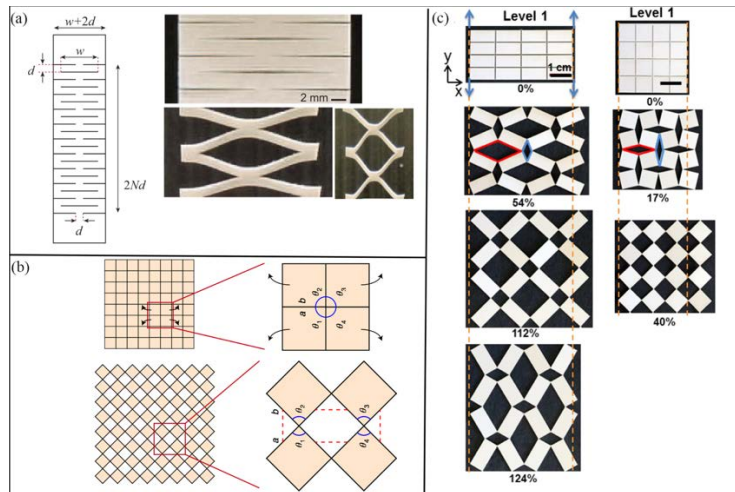


Figure 2.16 Different patterns of 2D kirigami: (a) with straight cuts [104], (b) a quad kirigami tessellation in closed and open forms [105] and (c) kirigami structures with square and rectangle cuts [35]

Figure 2.17 shows 3D kirigami patterns. The thickness of hinges and sheets has an impact on kirigami responses when it is exposed to uniaxial tension (Figure 2.17 a and b) [105], [106]. In specific conditions, the hinges respond out-of-plane buckle, and therefore, 3D geometry forms. In addition, it is possible to reproduce a particular 3D kirigami pattern by controlling the geometric parameters (Figure 2.17c) [107]. Figure 2.17d shows that a 2D kirigami structure can be converted to a 3D kirigami structure by applying a compressive force [108]. In this method, a part of the 2D



kirigami structure is attached to a pre-strain elastomeric substrate. When the substrate is released, the compressive force is applied to the structure. This causes out-of-plane buckling by which the structure transfers to a 3D kirigami structure [108].

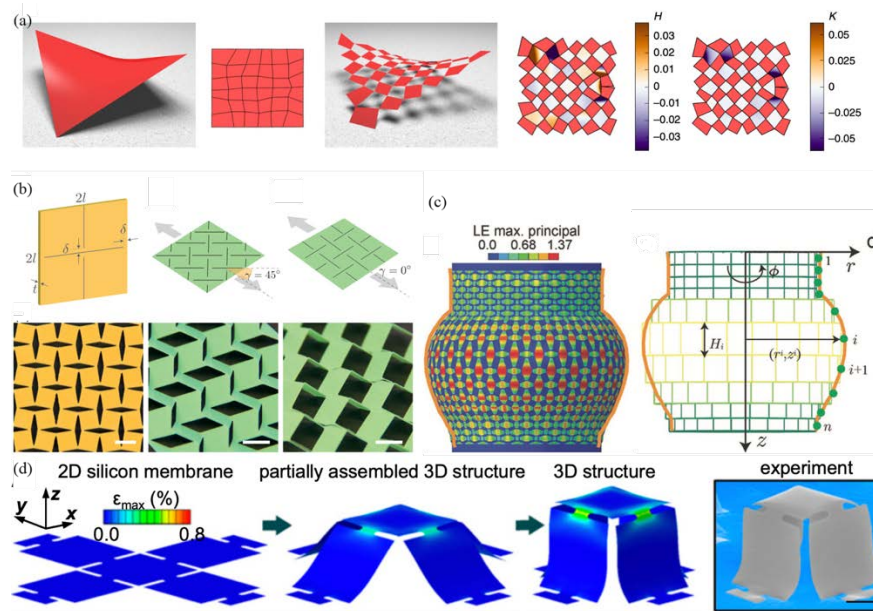


Figure 2.17 3D kirigami structures: (a), (b) 3D kirigami creation from out-of-plane buckling [105], [106], (c) controlling parameters of geometry to make 3D kirigami structure [107], and (d) compression buckled for designing 3D kirigami structure [108]

Kirigami pattern is an alternative method for making auxetic metamaterials. Auxetic materials show a negative Poisson's ratio. Poisson's ratio " $\nu$ " is the ratio of transverse strain " $\epsilon_t$ " to longitudinal strain " $\epsilon_l$ " when a material is stretched [103]. Most materials such as metals, polymers, and ceramics shrink when stretched longitudinally (positive Poisson's ratio). Figure 2.18 shows bistable auxetic mechanical metamaterials [103]. Bistable metamaterials have stability when the stretching force is released and keep their expanded geometry [109].

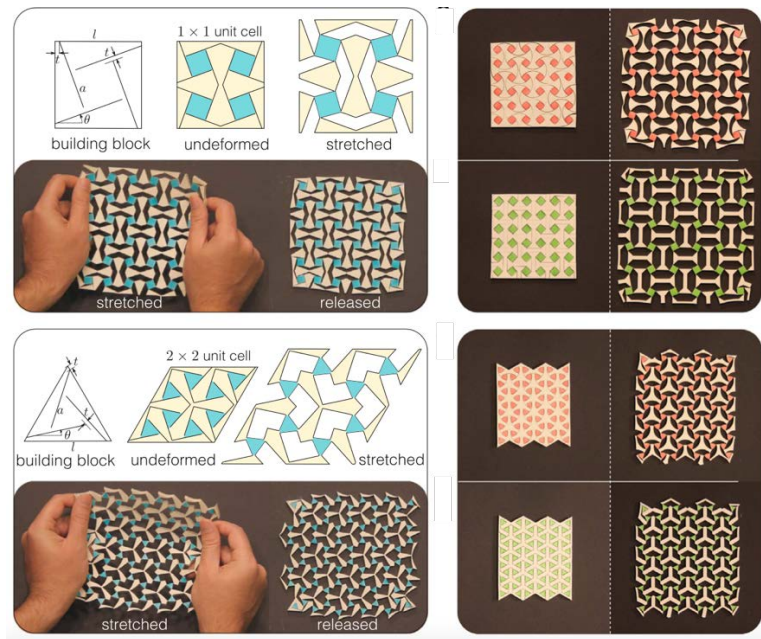


Figure 2.18 Bistable auxetic kirigami structures [103]

## 2.2 Application of kirigami structure in electronic devices

The capability of kirigami structures in adjusting geometry makes them suitable for stretchable and wearable electronics in different ranges of applications such as sensors [110], nanogenerators [126], biomimetic robotics [76], and energy storage devices [112].

In addition to stretchability, the robustness of materials properties during stretching is essential [113]. In different studies, the stability of kirigami structured materials was investigated [114]–[116]. For example, Guan et al. [43] fabricated stretchable kirigami-inspired conducting polymer based on poly(3-butylthiophene-2,5-diyl) (P3BT) nanowires and poly[(9,9-dioctylfluorenyl-2,7-diyl)-co-(4,4'-(N-(4-sec-butyl phenyl)diphenylamine))] (TFB) matrix. This kirigami structured composite showed electrical and mechanical durability after 1000 cyclic stretching at 2000% strain.

### 2.2.1 Sensors

Metamaterials contain repetitive and homogeneous parts. High quality and small form factors make them suitable for sensing applications [110]. Diao et al. [117] developed a kirigami-based humidity

dosimeter using PEDOT nanofibers. The sensitivity of this device was higher than the commercial PEDOT: PSS.

Kirigami structure is also used for durable and stretchable photodetector. For example, the performance of honeycomb-inspired kirigami photodetector made by PDMS/zinc oxide (ZnO) NWs was stable for more than 125% stretching and showed a fast recovery time of 100 ms [118]. In another study, Kim et al. [119] used the kirigami concept to design a UV photodetector based on ZnO nanorod decorated Au/polyvinylpyrrolidone nanofibers. The photodetector had stability for 50 stretching/releasing cycles at 80% strain.

In addition, kirigami structured devices have been extensively studied as strain sensors [120]–[122]. For example, Zheng et al. [123] fabricated a strain sensor by kirigami structured MoS<sub>2</sub> on PDMS. The stretchability of the strain sensor increased from 0.75% for the non-kirigami one to 15% for the kirigami structure.

## **2.2.2 Energy conversion and energy storage devices**

Providing energy is important for wearable electronic devices. Several strategies have been suggested to make wearable electronics, but the main issue is the mechanical compatibility of electronic devices and soft power sources. Therefore, stretchable energy conversion and energy storage devices have attracted researchers' attention in these fields.

There are many studies in kirigami structured energy conversion and storage devices such as kirigami structured nanogenerators [111], supercapacitors [117], and lithium-ion batteries (LIBs) [124].

Kirigami patterns have been used for a wide range of nanogenerators. Sun et al. [125] applied kirigami cuts on a thin poly(vinylidene fluoride) (PVDF) film to make a stretchable piezoelectric nanogenerator. The kirigami pattern decreased the piezoelectric performance of the kirigami-structured nanogenerator [125], [126]. Zhou et al. [39] reduced the effect of kirigami cuts on piezoelectric nanogenerators using T-joints cuts and improved stretchability by 300%. In addition, the kirigami structure was used for triboelectric nanogenerators by Wu et al. [127].

In addition to energy harvesting, kirigami patterns are a promising candidate to fabricate deformable energy storage devices. For example, a kirigami structured supercapacitor based on

MnO<sub>2</sub> NW composite showed 500% stretchability without reducing the electrochemical performance [128].

Stretchable LIBs are another choice as power suppliers for wearable electronic devices. For example, Bao et al. [129] designed a kirigami structured LIB, which was stretchable under 100% strain, and the resistance was stabilized under 30% strain during 500 stretching/releasing. In another study, Song et al. [130] manipulated both folds and cuts (i.e., origami and kirigami) to improve the stretchability of LIB.

In conclusion, kirigami patterns can improve stretchability and deformability due to their specific geometry. Therefore, kirigami structured devices are favorable for wearable electronics, especially health monitoring and biomedical applications.

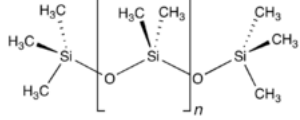
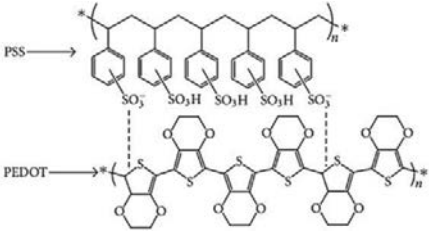
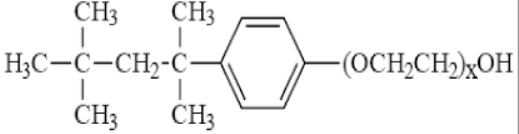
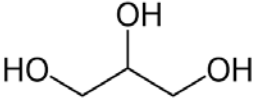
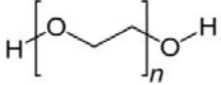
## CHAPTER 3 MATERIALS AND METHODS

This chapter explains the materials and methods used for this project.

### 3.1 Materials

Polydimethylsiloxane (PDMS, Sylgard 184 silicone elastomer kit) was purchased from Dow Corning. PEDOT:PSS (Clevios PH1000) was purchased from Heraeus Electronic Materials GmbH (Leverkusen, Germany). PEDOT:PSS screen printing paste (Clevios<sup>TM</sup>S V3 STAB) was purchased from Heraeus (Germany). P-t-octylophenol (Triton<sup>TM</sup> X-100, laboratory grade), and polyethylene glycol 400 were purchased from Sigma Aldrich. Glycerol (99.5 + % purity) was purchased from Caledon Laboratories Ltd (Georgetown, ON). Table 3-1 shows the chemical structure of the abovementioned materials.

Table 3-1 Chemical structure of used materials

Material	Chemical structure	References
PDMS		[131]
PEDOT:PSS (Clevios PH1000) and screen printing paste (Clevios <sup>TM</sup> S V3 STAB)		[132]
Triton <sup>TM</sup> X-100		[133]
Glycerol		[132]
Polyethylene glycol		[132]

## 3.2 preparation of non-kirigami films

The non-kirigami samples were rectangular with dimensions of 45 mm × 15 mm and 1 mm thickness.

### 3.2.1 Fabricating PEDOT: PSS/PDMS polymer composite films

Polydimethylsiloxane (PDMS) was prepared in a pre-cleaned glass Petri dish by mixing Sylgard-184 (Dow Corning) pre-polymer and a curing agent at a w/w ratio of 10:1 and degassed using a Centrifuge mixer at 2000 rpm for 5 minutes. Next, to prepare PEDOT:PSS/PDMS composite polymer film, 0.35 g PEG-400 (as plasticizer), 0.5 g Triton X-100 (for better miscibility) [133], 0.5 g glycerol (for increasing electrical conductivity) [132] and 5 g PEDOT:PSS (Clevios PH1000)

were mixed with PDMS mold at 2000 rpm for 30 min using the same Centrifuge mixer. Then, the mixture was poured into a precleaned glass Petri dish and cured gradually at 60 °C for 6 h to avoid bubble formation in the resultant films (Figure 3.1).

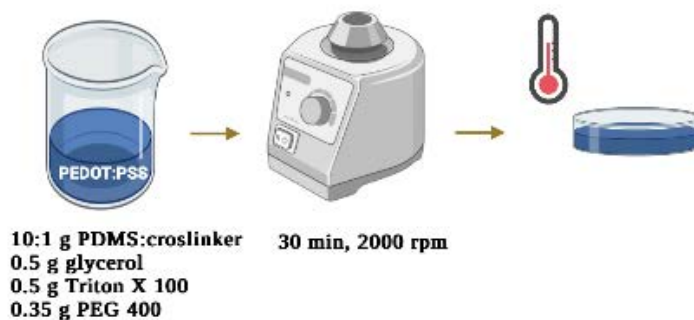


Figure 3.1 Fabrication of PEDOT:PSS/PDMS polymer composite film

### 3.2.2 Fabrication of PEDOT:PSS coated PDMS

The Polydimethylsiloxane (PDMS) substrate was prepared by mixing the monomer dimethylsiloxane and its crosslinker in the ratio of 10:1 (weight by weight). The resultant mixture was degassed using a Centrifuge mixer at 2000 rpm for 3 minutes to remove any air bubbles. Then the mixture was poured into a circular-shaped glass container with 10 cm diameter, which was thoroughly cleaned with acetone, isopropanol (IPA), distilled water and was dried using an air gun. A solution of 5 mM of cetyltrimethylammonium bromide (CTAB) in deionized water was applied to the glass mold to easily remove the PDMS substrate. Next, the mixture was carefully poured into the precleaned mold. The average thickness of the PDMS substrate was 1 mm for kirigami structure cuts. For the curing process, the mixture was covered with a cap to keep it away from contaminants. It was cured by keeping it on a hot plate at 100 °C for 1 hour. PDMS substrate was then removed using a surgical blade. Prior to PEDOT:PSS deposition onto PDMS, the substrate underwent UV/Ozon treatment for 20 minutes to make its surface hydrophilic. Subsequently, PDMS samples were coated once with PEDOT:PSS solution and ink using a glass slide and then cured at 100 °C for 1 hour (Figure 3.2).

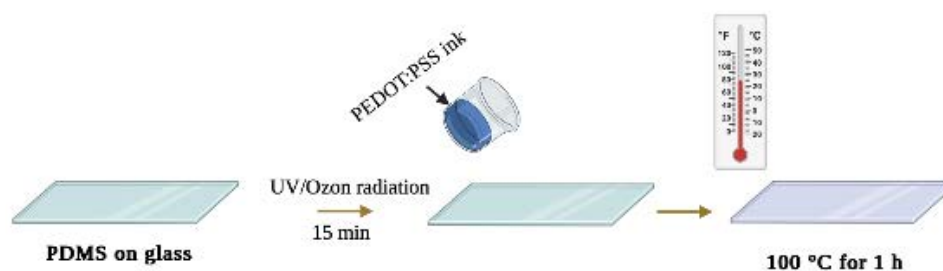


Figure 3.2 Fabrication of kirigami structured PEDOT:PSS coated PDMS film

### 3.3 Preparation of Kirigami structured specimens

The kirigami pattern [103], [109] was plotted by AutoCAD software [134]. The kirigami specimens were prepared by creating patterns on non-kirigami films using a 100 W laser cutter with a speed of 10 mm/s and 25% power. The kirigami structured samples had hexagonal geometry with 70 mm  $\times$  50 mm  $\times$  1 mm dimensions. It is worth mentioning that for preparing the kirigami structured PEDOT:PSS coated PDMS specimen, the PDMS film was laser cut before coating with PEDOT:PSS ink.

### 3.4 Scanning electron microscopy (SEM)

Scanning electron microscopy (SEM) is a kind of microscopy technique for observing the morphology of materials by surface scanning of materials using an electron beam. When the electron beam is incident on a surface, different signals are produced. The produced signals contain secondary, back-scattered, transmitted, and absorbed electrons. The secondary electrons have information about surface topography, which the detector can detect. This technique of observing microstructures and morphologies is ubiquitous in many fields of study, whether materials science, electronics, or biology [135]. Different elements of SEM are shown in Figure 3.3.



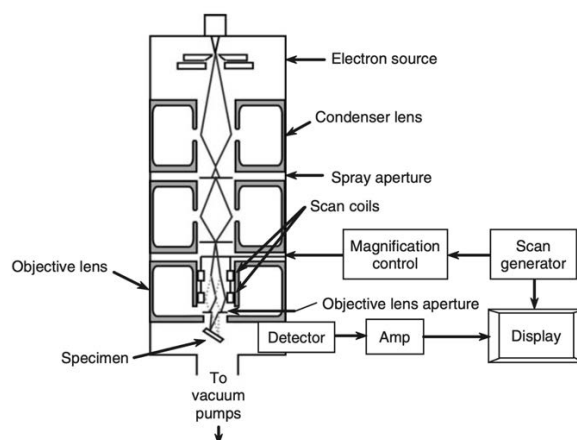


Figure 3.3 Different parts of SEM [135]

### 3.5 Optical microscopy

The optical microscope is the oldest and simplest microscope that uses visible light and a set of lenses to magnify images of samples. Recent optical microscopes capture digital images by charged-coupled devices (CCDs). Figure 3.4 shows different parts of an optical microscope [136].

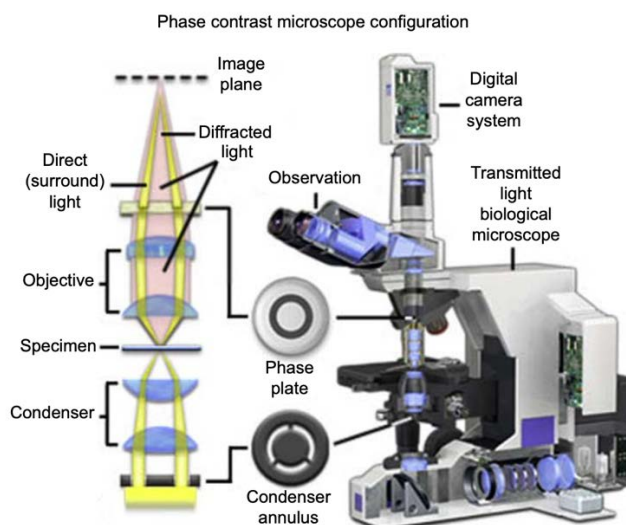


Figure 3.4 Different parts of an optical microscope [139]

The surface morphology of PEDOT:PSS deposited on the PDMS substrate was evaluated using an optical microscope (Zeiss Axiocam 105) and a scanning electron microscopy (SEM) (Hitachi TM3030).

## 3.6 Mechanical Properties

A multi-axial mechanical tester (Mach-1 model v500csst, Biomomentum, Canada) was used to characterize the mechanical properties of kirigami structured specimens and non-kirigami films. The applied force was measured using a standard load cell of 70 N.

### 3.6.1 Tensile strength

Uniaxial tension was applied to specimens at a speed of 0.1 mm/s to investigate the tensile strength of samples. The test was repeated three times to calculate the average values and standard deviations of Young's modulus and elongation at break from force-displacement curves.

#### 3.6.1.1 Young's modulus and elongation at break

Young's modulus is the ratio between uniaxial stress to strain. It is also defined as elastic modulus or tensile modulus and describes relative stiffness [137], [138]. Young's modulus ( $E$ ) can be obtained from force-displacement curves from Eq. (3-1):

$$E = \frac{\text{Slope} \times \text{film thickness}}{\text{film area}} \quad (3-1)$$

where the slope is obtained from the elastic region of the force curve.

Elongation at break exhibits the strength of material to break. It is defined as fracture strain and is obtained from change in the length of material at break point to initial length as Eq. (3-2) [72]:

$$\text{Elongation} = \varepsilon = \frac{\Delta L}{L} \times 100 \quad (3-2)$$

### 3.6.2 Viscoelastic behavior

When stress is applied to materials, the viscoelastic behavior causes elastic strain and time-dependent or viscous strain [140]. The elastic behavior is derived from the change of chain length and angle. Viscous behavior causes plastic deformation in materials when a uniaxial strain is

applied. Plastic deformation is related to molecular orientation and crystalline phase movement [141].

In this project, the viscoelastic behavior of samples was studied by analyzing the measurements obtained from cyclic and dynamic mechanical tests.

### 3.6.3 Behavior in cyclic test

To study recovery behavior, samples are exposed to loading-unloading. Figure 3.5 shows the recovery curve of a material [142]. When the applied stress is removed, the ability of materials to come back to their initial position is called elastic recovery. Elastic strain is recoverable, but the viscous elastic is reverse [141].

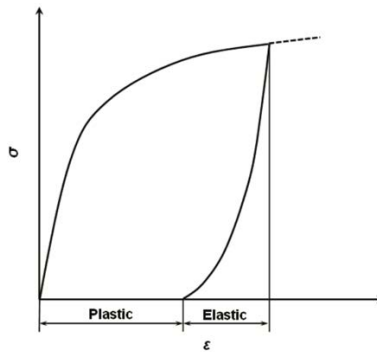


Figure 3.5 The stress-strain and recovery curves of a material [141]

The elastic recovery or strain recovery can be obtained from Equation (3-3).

$$\text{Elastic recovery} = \frac{\text{Elastic strain}}{\text{Total strain}} \quad (3-3)$$

Moreover, work recovery is another factor for studying tensile deformation. When strain is applied to a material, the total work done is either stored in chemical bonds or lost in the form of heat. The stored work in chemical bonds appears as elastic strain and is recoverable. The work lost appears as plastic deformation and is not recoverable. The work recovery is obtained as Equation (3-4):

$$\text{Work recovery} = \frac{\text{Work returned during recovery}}{\text{total work done during stretching}} \quad (3-4)$$

In this work, the cyclic tests were carried out by applying different pre-strains (25%, 35%, 45% and 55%) at a constant axial strain rate of 1 mm/s and room temperature. In addition, the cyclic loading/unloading tests were conducted at 25% strain for 500 cycles. 500 is a large enough number to have a stabilized response. At 25% strain, the kirigami structured specimens opened entirely.

### 3.6.4 Dynamic tests

The dynamic test was performed by applying axially sinusoidal strain on non-kirigami and kirigami structured samples at a frequency equal to 0.5 Hz, speed rate of 1mm/s and room temperature.

In viscoelastic materials, strain can be written as Eq. (3-5) [142]:

$$e = e_0 + e_m \sin \omega t \quad (3-5)$$

where “ $e_0$ ” is the strain at  $t=0$ , “ $e_m$ ” is strain amplitude equal to 10 mm, and “ $\omega$ ” is the angular frequency in rad/s.

Stress is calculated from Eq. (3-6) [142]:

$$S = S_0 + S_m \sin(\omega t + \delta) \quad (3-6)$$

where “ $S$ ” is stress at  $t=0$ ,  $S_m$  is stress amplitude and “ $\delta$ ” is angular phase difference or loss angle between stress and strain [142]. The value of “ $\delta$ ” is also expressed as a delay between the applied strain and stress.

### 3.6.5 Electromechanical test

Electromechanical responses were recorded when the samples were subjected to different strains until they broke entirely, as well as 5000 loading/unloading cycles at 25% strain. Electromechanical properties were measured using a customized uniaxial translational manipulator coupled with electrical equipment (Agilent B2902A) in a constant voltage mode.

## CHAPTER 4 RESULTS AND DISCUSSION

### 4.1 Kirigami pattern

Kirigami-based metamaterials have monolithic periodic structures with tunable properties such as stiffness, auxeticity, and bistability [143]. The auxetic structure shows a negative Poisson's ratio. The auxetic structures offer stretch perpendicular to stress due to their microstructure [144], [145]. Bistability means the structure can maintain its deployed state when the load is removed. When the auxetic structure opens, the rotation of units leads to snap-through instabilities. This phenomenon makes the structure auxetic and bistable [103]. In this work, we used a triangular bistable auxetic structure by perforating parallel cut motifs already reported in the literature [103] (Figure 1a (I)). In this structure, the length of the rotating unit was half of the building block ( $a/l = 1/2$ ,  $l = 20 \text{ mm}$ ). Also, the size of the ligament between cuts and the edge lengths was  $t=1 \text{ mm}$  (Figures 1a(II) and (III)). Photographs of the kirigami structured PEDOT:PSS coated PDMS and polymer composite in closed and open forms are shown in Figures 4.1(b, c) and (d, e), respectively.

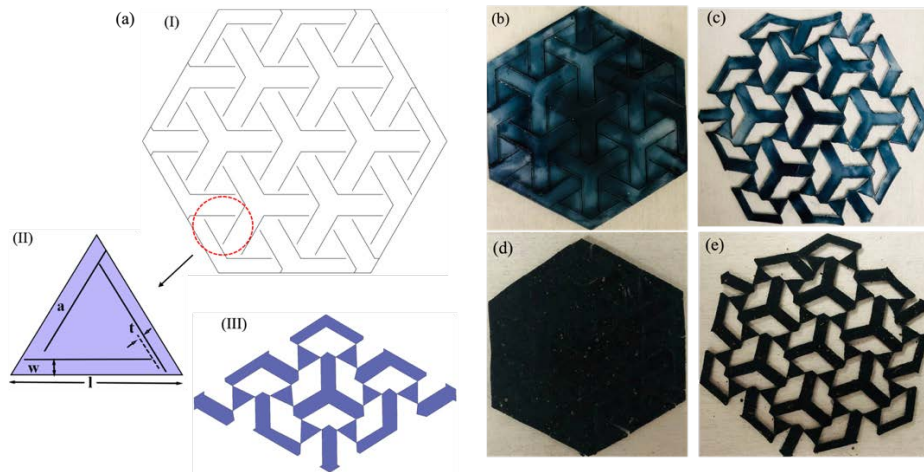


Figure 4.1 (a) *I*: Schematic of kirigami structure in closed form, *II*: the dimensions of the rotating unit and *III*: the schematic of one building block in open form; photographs of kirigami structured PEDOT:PSS coated PDMS specimen (b) in closed and (c) open forms; photographs polymer composite specimen in (d) closed and (e) open forms.

## 4.2 Mechanical properties

### 4.2.1 Tensile strength

Uniaxial tension was applied to specimens to investigate their tensile strength. The mechanical behavior of non-kirigami films was also studied for comparison (Figure 4.2a). Under monotonic stretching, non-kirigami specimens show a nonlinear stress-strain relationship. As Figure 4.2a shows, the non-kirigami PDMS film has a higher tensile strength than non-kirigami PEDOT:PSS coated PDMS and polymer composite films. In addition, the serrated region in non-kirigami PEDOT:PSS coated PDMS film was because of the cracks formed on the surface of PEDOT:PSS coating by applying stress. The results in Figure 4.2b show that the force-displacement curves comprise two parts, i.e., a smooth region (part I) followed by a serrated region (part II). Beyond the smooth area, the serrated region occurred when individual hinges of the kirigami specimen started to break. The Young's modulus ( $0.21 \pm 0.025$  MPa) decreased in the non-kirigami polymer composite film in comparison to non-kirigami PEDOT:PSS coated PDMS film ( $2 \pm 0.12$  MPa) and non-kirigami PDMS film ( $\sim 0.75 \pm 0.035$  MPa) (Figure 4.2c). The Young's modulus and elongation at break of kirigami structured specimens followed the same trend as the non-kirigami films. The Young's modulus of kirigami structured specimens decreased compared to non-kirigami ones (Figure 4.2c). On the contrary, the elongation at break increased in kirigami structured specimens. Furthermore, the elongation at break of non-kirigami and kirigami structured PEDOT:PSS/PDMS composite film was more than non-kirigami PDMS and PEDOT:PSS coated PDMS films. PEG in the polymer composite acted as a plasticizer [132] and increased elongation at break to  $\sim 108\%$  (Figure 4.2d). In addition, PDMS doping with Triton X-100 increased adhesion and in consequence, improved stability (elongation at break) [133]. Therefore, it can be concluded that coating PDMS with PEDOT:PSS decreased tensile strength as well as stretchability. The Young's modulus and elongation at break of kirigami structured specimens followed the same trend as the non-kirigami films. For the kirigami structured polymer composite, the elongation at break was 15% more than the elongation at break for the kirigami structured PDMS specimen; it was also 41% more than the elongation at break of the kirigami structured PEDOT:PSS coated PDMS specimen (Figure 4.2d).

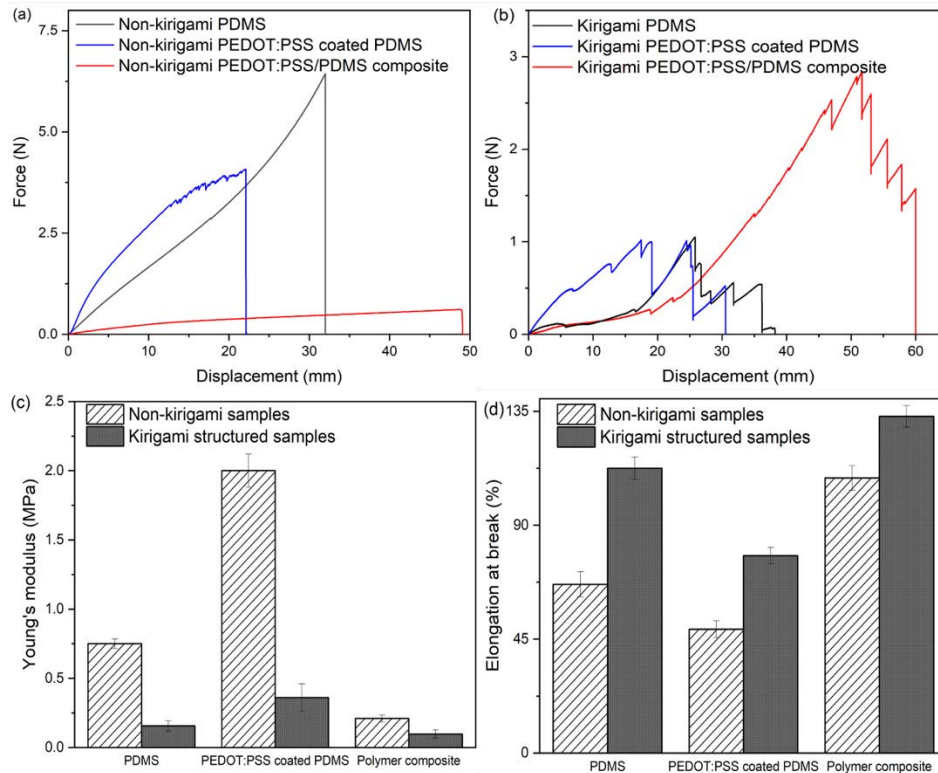


Figure 4.2 (a) force-displacement curves of non-kirigami films; (b) force-displacement curves of kirigami structured specimens; (c) Young's modulus and (d) elongation at break of non-kirigami and kirigami structured specimens

#### 4.2.2 The behavior of specimens in cyclic tests

Figure 4.3 shows one cyclic loading/unloading of samples at different strains (25%, 35%, 45% and 55%). The plastic deformation (i.e., residual strain) was zero for one loading/unloading cycle for the abovementioned strains. In addition, we noticed Mullin softening effect because of structural damages [146] when cyclic uniaxial tension was applied at various stretching levels. This effect means when elastomeric materials are subjected to tension, the stress required for reloading is less than the initial stress at the first loading [147].

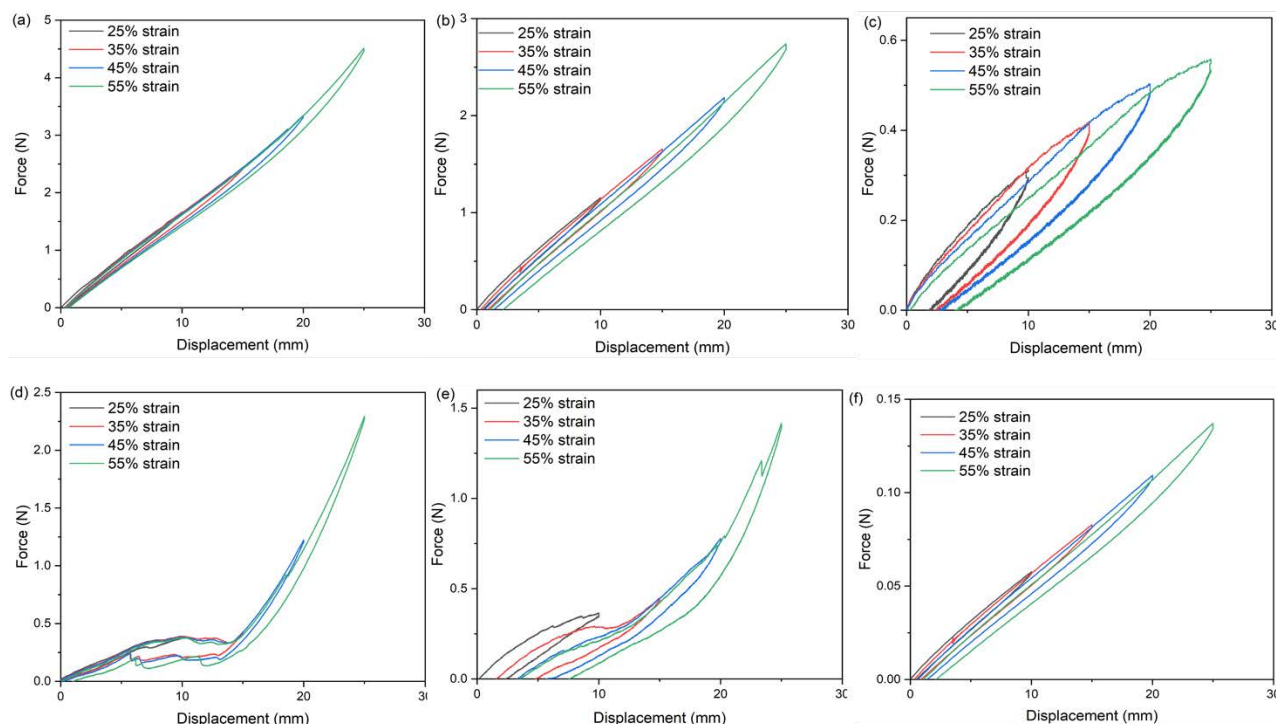


Figure 4.3 Loading/unloading curves under 25%, 35%, 45% and 55% strain for simple (a) non-kirigami) PDMS films, (b) non-kirigami PEDOT:PSS coated PDMS films, (c) non-kirigami polymer composite films, (d) kirigami structured PDMS specimens, (e) kirigami structured PEDOT:PSS coated PDMS specimens, and (f) kirigami structured polymer composite specimens

In this project, energy loss was calculated when the samples were subjected to a loading/unloading cycle up to a maximum applied strain of 25% at a 0.1 mm/s strain ratio. As shown in Figure 4.4, the energy loss manifested as a hysteresis loop when the kirigami structured specimens were cycled between 0 to 25% strain. Although the hysteresis loop can be related to molecular network reorientation [148], the kirigami structured specimens did not experience significant plastic deformation when subjected to loading/unloading up to 25%. The area inside the hysteresis loop represents the energy loss. Therefore, the larger the area inside the curve is, the higher the energy loss will be. By calculating the area of each loop by MATLAB software [149], [150], we noticed energy dissipation in the kirigami structured PEDOT:PSS coated PDMS specimen was less ( $\sim 0.46$  J) than the energy dissipation of the non-kirigami ones ( $\sim 15$  J). A similar result was obtained for the polymer composite samples. The energy loss for the non-kirigami polymer composite was  $\sim 0.73$  J, while for the kirigami structured polymer composite, it was  $\sim 0.3$  J (Figure 2S).



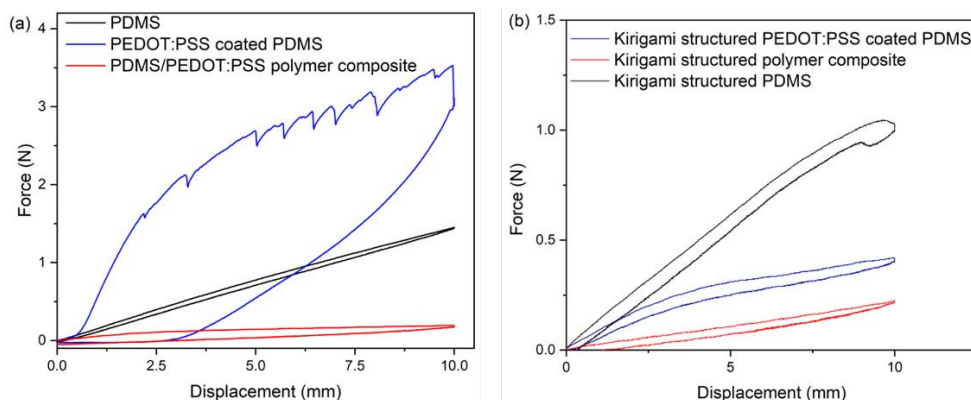


Figure 4.4 Loading and unloading curves of (a) simple (non-kirigami) and (b) kirigami structured PDMS, PEDOT:PSS coated PDMS, and polymer composite at 25% strain

To study the viscoelastic behavior of samples under cyclic deformation, each sample was exposed to 500 loading/unloading cycles at 25% strain, strain ratio of 1 mm/s (3 h), and room temperature. The materials showed stress softening and hysteresis loops due to their viscoelastic properties and microstructural damages that occurred during loading [151]. In comparison to initial stress, the stress in the second cycle dropped and remained approximately constant for the rest of the cycles (Figure 4.5).

The viscoelastic effect in samples appeared as plastic deformation (i.e., residual strain). After 500 loading/unloading cycles, the residual strain was less than 1% for the kirigami structured polymer composite, 2.5% for the kirigami structured PEDOT:PSS coated PDMS, and 2% for the kirigami structured PDMS. On the other hand, the residual strain for the non-kirigami PEDOT:PSS coated PDMS, polymer composite and PDMS films were  $\sim$  5%, 2.25% and 3.5%, respectively. As a result, the kirigami structured samples showed more elastic behavior than non-kirigami samples.

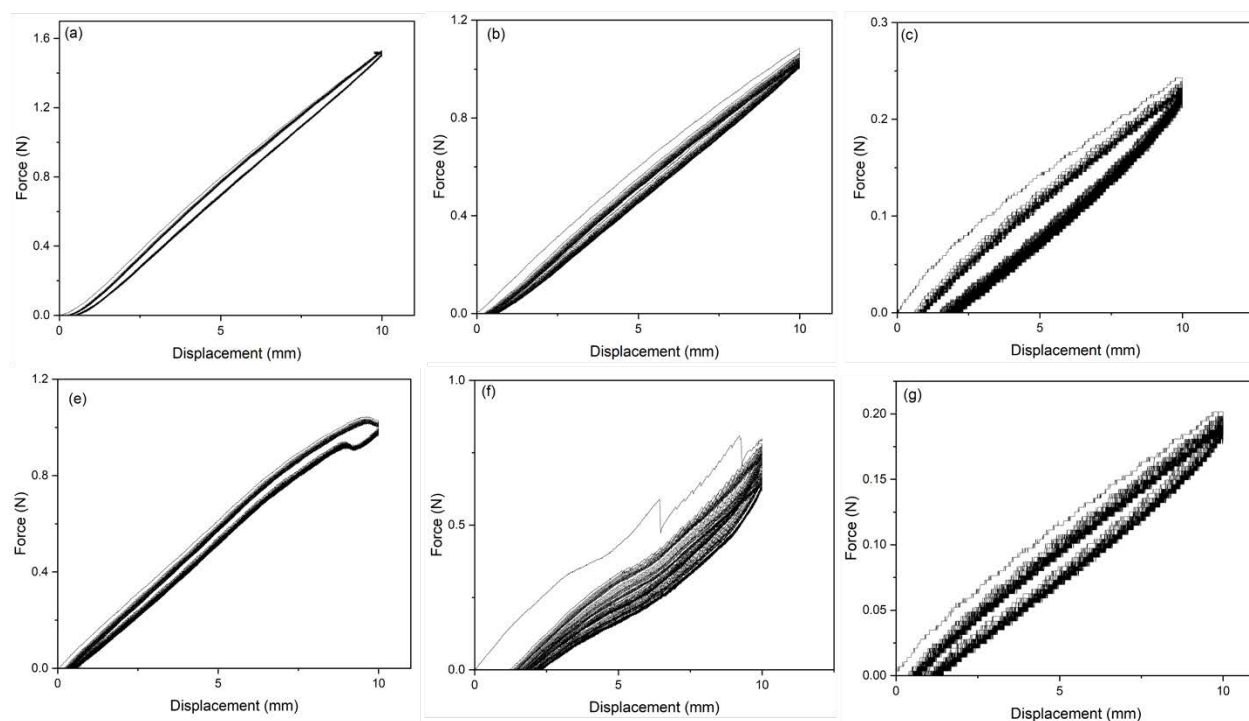


Figure 4.5 50 cycles of loading/unloading under 25% strain at a strain ratio of 1 mm/s and room temperature for (a), (b), (c) non-kirigami and (e), (f), (g) kirigami structured PDMS, PEDOT:PSS coated PDMS and polymer composite, respectively

Moreover, the energy dissipation decreased by increasing the number of cycles [152]. As figures 4.6a and 4.6b show, the energy dissipation stabilized after a certain number of loading/unloading cycles. For example, the energy dissipation in the kirigami structured polymer composite was constant after the third cycle, but in kirigami structured PDMS and kirigami structured PEDOT:PSS coated PDMS, it was constant after 100<sup>th</sup> cycles and 250<sup>th</sup> cycles, respectively. A similar result was demonstrated for non-kirigami structured samples. However, in the non-kirigami structured PEDOT:PSS coated PDMS, the energy dissipation decreased dramatically in the 150<sup>th</sup> cycle and was uniform until the 250<sup>th</sup> cycle. These results show that by increasing the number of loading/unloading cycles, the energy stored in polymer chains became constant. Also, the intermolecular interactions between the polymer chains decreased. This might result in configuration changes. Therefore, the behavior of samples was close to elastic behavior at the last cycles.

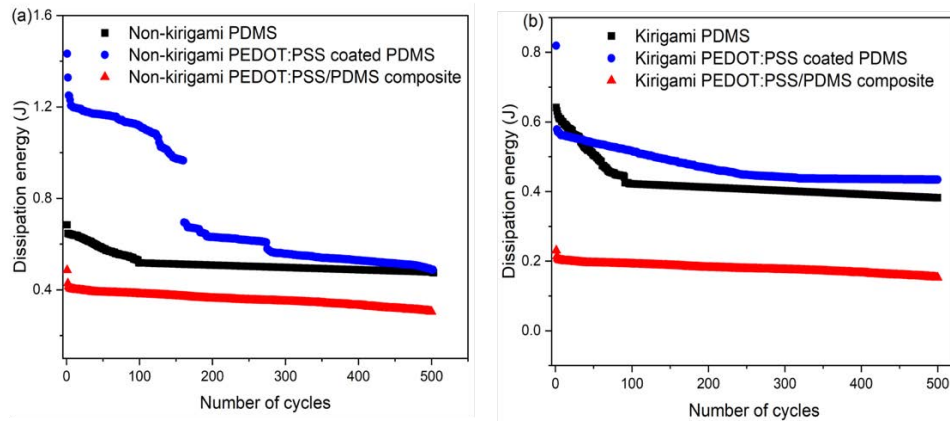


Figure 4.6 Energy dissipation for 500 loading/unloading cycles for (a) non-kirigami and (b) kirigami structured samples

### 4.2.3 Properties of specimens under dynamic mechanical test

Dynamic mechanical properties are usually expressed as complex dynamic modulus ( $E^*$ ) containing storage modulus ( $E'$ ) and loss modulus ( $E''$ ). The storage modulus represents the material's stiffness, while the loss modulus is attributed to the loss of energy within the material through plastic deformation, morphology changes, and molecular motion. Complex modulus, storage modulus ( $E'$ ), and loss modulus are obtained from Eq. (4-1), Eq. (4-2), and Eq. (4-3), respectively [142].

$$E^* = \frac{S_m}{e_m} = f_m/A \times L/\Delta L \quad (4-1)$$

where " $f_m$ " is force amplitude, " $A$ " is sample area, " $L$ " is the length of the sample and " $\Delta L$ " is displacement.

$$E' = \frac{S_m}{e_m} \cos \delta \quad (4-2)$$

$$E'' = \frac{S_m}{e_m} \sin \delta \quad (4-3)$$

The loss factor ( $\tan \delta$ ) is calculated from the ratio between  $E'$  and  $E''$  [142].

As Figure 4.6 shows, all samples showed a delay by applying strain ( $\delta$ ), which confirmed viscoelastic behavior. When the strain was applied to the samples, the force increased, and its value was positive. On the contrary, the negative values in sinusoidal force are represented as stress relaxation and associated with the released strain. In addition, for the non-kirigami samples, some of the applied strain was stored in polymer chains; therefore, the force became constant. In contrast, for the kirigami structured samples, the force decreased until the next period of strain was applied. This means that the applied force was released completely. From these results, it can be concluded that the kirigami structured samples had more elastic behavior than the non-kirigami samples.

Table 1 reports the values of " $\delta$ ", " $\tan\delta$ ", " $E^*$ ", " $E'$ ", and " $E''$ ". As shown in Table 1, the storage modulus and loss modulus decreased for the kirigami structured samples. Decrease in storage modulus means decrease in materials' stiffness. Therefore, materials with less storage modulus have better stretchability. These results have good agreement with the previously mentioned results discussed for figures 4.5 and 4.7. In addition, the delay of materials to respond to applied strain ( $\delta$ ) decreased in the kirigami structured samples.

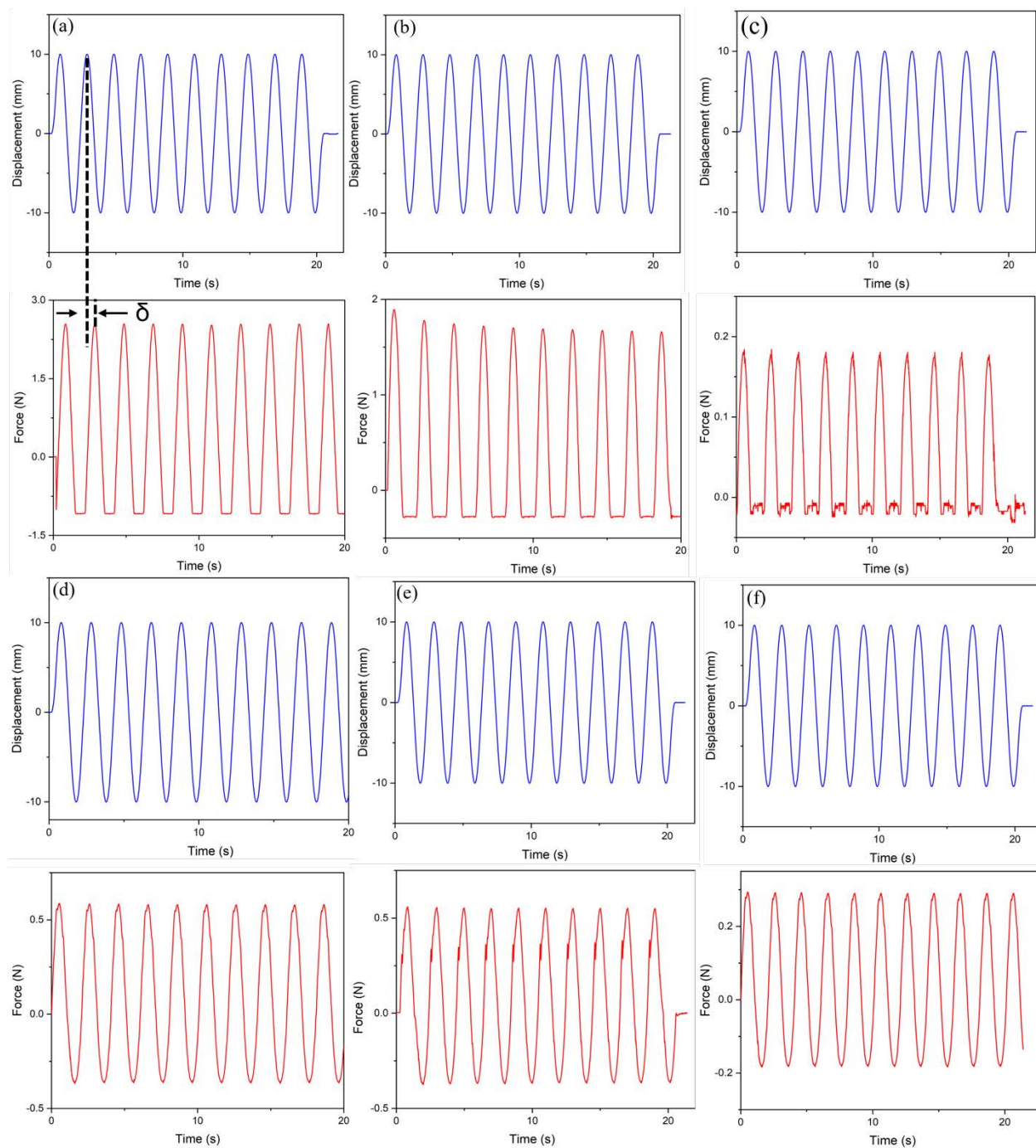


Figure 4.7 Sinusoid curves displacement-time (in blue) and force-time (in red) for non-kirigami (a) PDMS, (b) PEDOT:PSS coated PDMS and (c) polymer composite films versus sinusoid curves displacement-time (in blue) and force-time (in red) for kirigami structured (d) PDMS, (e) PEDOT:PSS coated PDMS, and (f) polymer composite specimens

Table 4-1 Values of  $\delta$ ,  $\tan\delta$ ,  $E^*$ ,  $E'$ , and  $E''$  for the non-kirigami samples and kirigami structured specimens

Sample	$E^*$ (MPa)	$E'$ (MPa)	$E''$ (MPa)	$\delta$ ( $^\circ$ )	$\tan\delta$
Non-kirigami PDMS film	0.762	0.759	0.059	4.400	0.0769
Non-kirigami PEDOT:PSS coated PDMS film	2.500	2.460	0.434	10.000	0.1763
Non-kirigami polymer composite film	0.252	0.251	0.010	2.300	0.04
Kirigami structured PDMS	0.144	0.144	0.005	2.100	0.0366
Kirigami structured PEDOT:PSS coated PDMS	0.293	0.293	0.017	3.400	0.0594
Kirigami structured polymer composite	0.088	0.088	0.002	1.500	0.0261

### 4.3 Electromechanical properties

The electromechanical properties of all samples were studied under varying applied strains (Figure 4.8). It was observed that when the non-kirigami structures were stretched beyond a critical value, both quasi-periodic cracks and wrinkles were formed (Figure 4.9). In general, cracks form because of inherent flaws within the materials and grow by channeling. In contrast, wrinkles form because of the Poisson ratio difference between the film and the strained substrate. As shown in Figure 4.8, these cracks and wrinkles in the non-kirigami samples were aligned in a direction perpendicular to each other. Crack density, crack width, wrinkle amplitude, and wrinkle wavelength increased in the non-kirigami films when the stretch increased (Figure 4.9). Quasi-periodic cracks and wrinkles disrupted the current pathways; hence, the current decreased with stretching. Upon the release of the stretched sample, the cracks connected partially and the current partly recovered its initial value. In the kirigami specimens, the current decreased in the open position. In addition, the current decreased with increasing strain and was equal to zero when the samples completely broke. In the

kirigami structured polymer composite specimen, the current could flow until 140% strain. Then, the specimen completely broke at 145% strain. The non-kirigami polymer composite broke at 125% strain. The generation of cracks and fractures near the hinges caused current reduction. However, the current reduced more in the non-kirigami polymer composite film than the kirigami structured specimens. For example, the initial current value of the non-kirigami polymer composite reduced to 44% in the closed form after 100% strain, but for the kirigami structured polymer composite specimen, the value decreased to  $\sim 29\%$ .

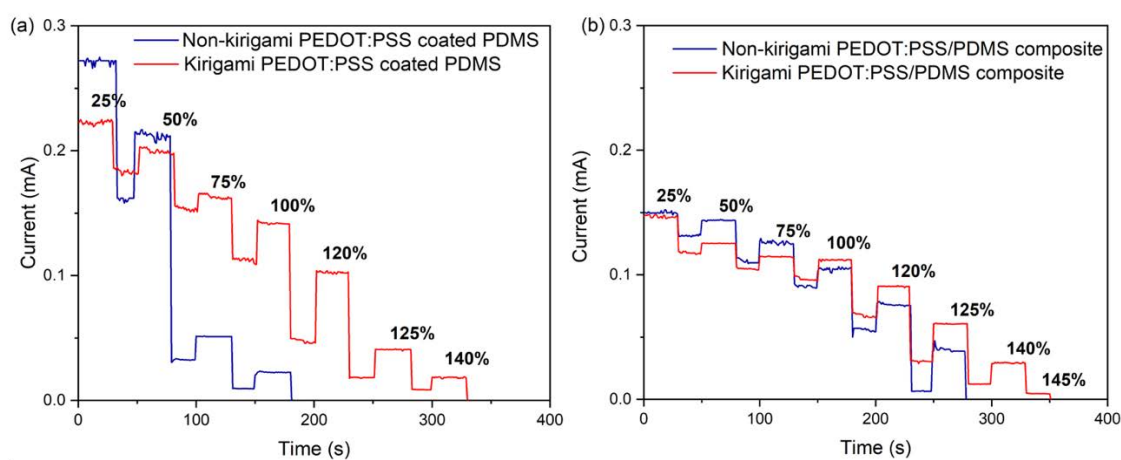


Figure 4.8 Current versus time at different applied strains for (a) non-kirigami and kirigami PEDOT:PSS coated PDMS and (b) non-kirigami and kirigami PEDOT:PSS/PDMS composite samples.

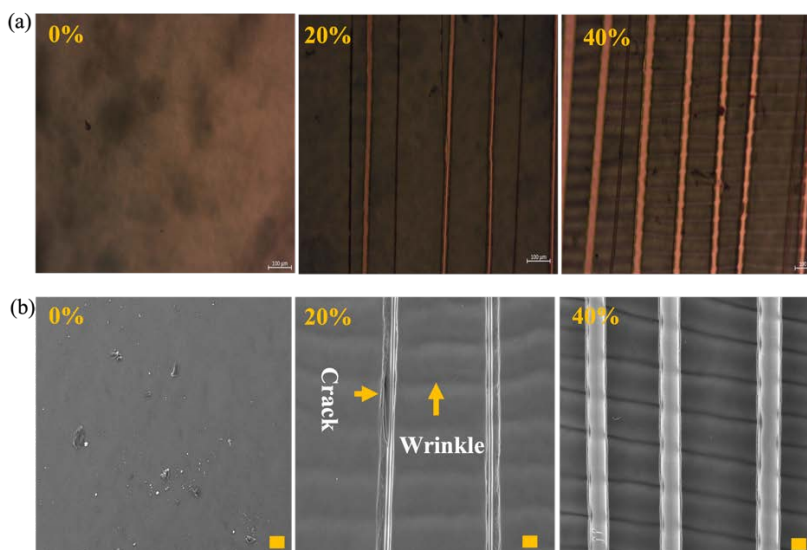


Figure 4.9 (a) Optical and (b) SEM images when samples were exposed to 0, 20% and 40% strain.

Figure 4.9 plots the current with respect to time under 1000 stretching/releasing cycles at 25% strain for the non-kirigami films. The current amplitude decreased by  $\sim 40\%$  at the beginning of stretching for the non-kirigami PEDOT:PSS coated PDMS film due to increased crack density, crack width, wrinkle amplitude, and wrinkle wavelength discussed in the previous section (Figure 4.10a). However, for the non-kirigami polymer composite film, the current decreased 10% under 5000 stretching/releasing cycles (Figure 4.10b).

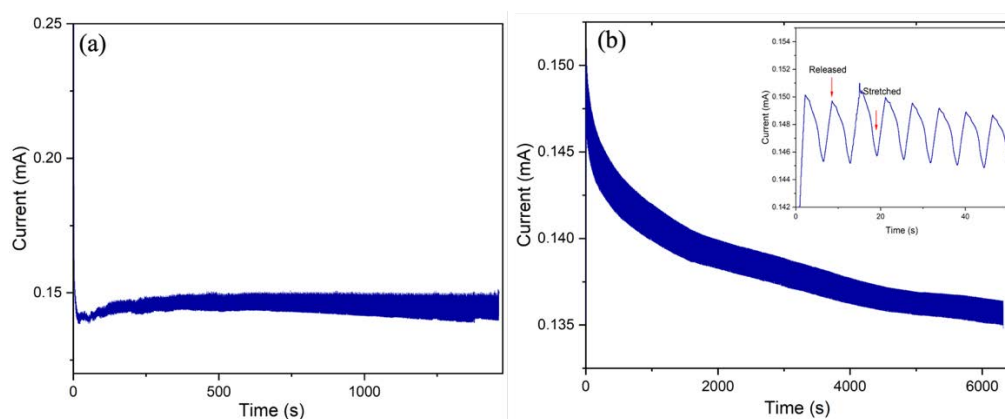


Figure 4.10 Current-time graphs of (a) non-kirigami PEDOT:PSS ink coated PDMS fil, and (b) non-kirigami polymer composite film at 25% strain under 1000 stretching/releasing cycles



The kirigami structured specimens were subjected to many opening/closing cycles, i.e., 5000 under a constant voltage of 10 mV (Figure 4.11). The original length of the sample was 4 cm in closed form and 5 cm (strain = 25%) in open form.

In the kirigami structured PEDOT:PSS coated PDMS samples, the current amplitude monotonically decreased as the strain progressed (Figure 4.11). To understand the overall behavior of the plot, the current amplitude values between open and closed forms were compared at first and 5000<sup>th</sup> cycles (~ 2.1 h). In the first cycle, the current amplitude changed from 0.23 mA at closed state to 0.21 mA at open state with the current change ( $\Delta I_{1st}$ ) of about 8.69%. The current amplitude reduced 30% after 1000 opening/closing cycles in the closed form. By considering the current amplitude of non-kirigami (discussed previously for Figure 4.10a) and kirigami structured PEDOT:PSS coated PDMS samples at 1000 opening/closing cycles, we can conclude that the electromechanical stability improved 10%.

For the kirigami structured PEDOT:PSS coated PDMS sample, the current amplitude was 0.101 mA in the closed-form and 0.0944 mA in the open form ( $\Delta I_{5000th} \approx 6.53\%$ ) after 5000 cycles. Therefore, the current amplitude reduced by 56% in closed form and 55% in the open form at the 5000<sup>th</sup> cycle. In the kirigami structure, PEDOT:PSS ink was well connected via hinges through which the charge carriers traveled across the whole perforated periodic structure. These hinges were aligned in different directions during opening/closing cycles with respect to the direction of external stretching. When the structure was opened and closed, an individual hinge experienced a certain strain. The total strain-induced elastic energy was redistributed among all the hinges. As a result, the correlation of elasticity and electrical transport in the kirigami-inspired structure is not straightforward. In addition, there was an elasticity mismatching at the interface between PEDOT:PSS and PDMS. So PEDOT:PSS ink and PDMS experienced different amounts of strain-induced force when the whole structure was exposed to an external strain. This process led to crack and wrinkle formation. The morphology of the PEDOT:PSS ink deposited on the kirigami-structured PDMS was investigated in the closed form (Figure 4S) and open form at three distinct positions (Figure 4.12). The shape and density of the cracks influenced the current flowing in the film under strain [132]. In the closed form, wrinkled and cracked areas were unclear, and the cracks were sharp in the edges where joints were connected. Regions 1 and 2 were subjected to more tension in the open form, so more cracks were observed. Region 3 contained wrinkles implying

this region was exposed to less stretching. Therefore, long size and high-density cracks partially interrupted the electrical conducting pathways during the stretching, resulting in current amplitude reduction [132].

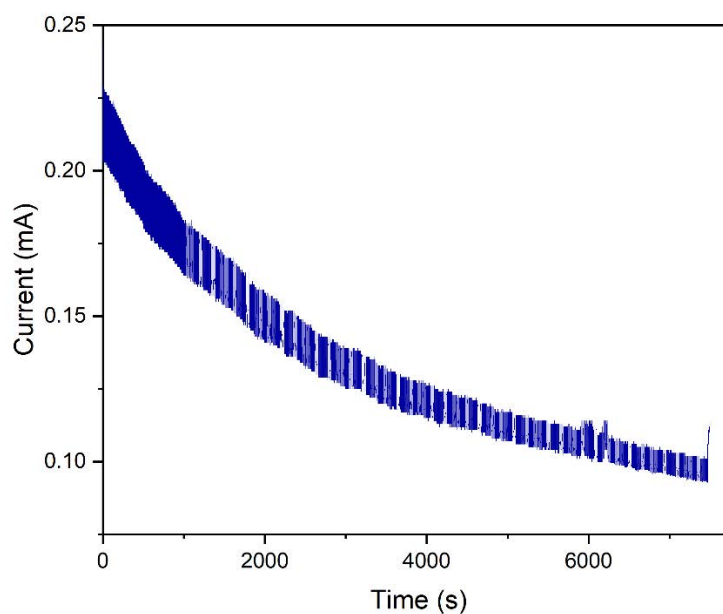


Figure 4.11 Current-time graphs for (a) complete period of 5000 opening/closing cycles, (b) initial, (c) 1000, and (d) 5000 opening/closing cycles for kirigami structured PEDOT:PSS ink coated PDMS specimen

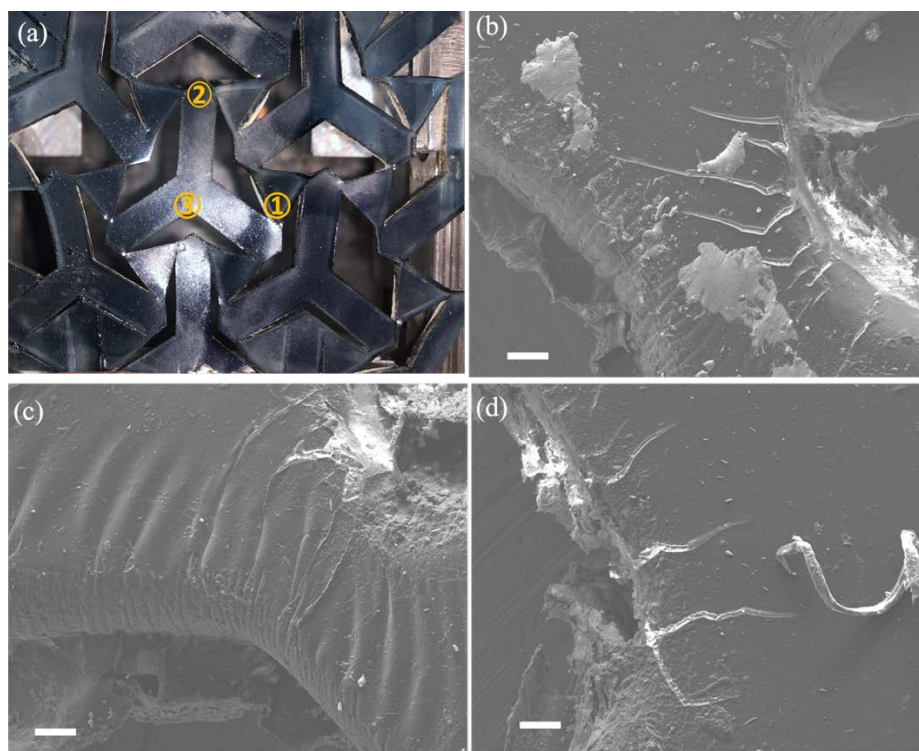


Figure 4.12 (a) photograph and SEM images of kirigami structured PEDOT:PSS coated PDMS specimen after 5000 opening/closing in the open form at the regions of (a) 1, (b) 2, and (c) 3. The scale bar is 100  $\mu\text{m}$ .

Figure 4.13 shows the current-time graphs of the kirigami structured polymer composite sample. The current amplitude remained approximately stable even during 5000 opening/closing cycles. Triton X-100 has a hydrophobic tail and a hydrophilic head [133]. As a result, Triton X-100 was connected to PDMS by the hydrophobic part and linked to PEDOT:PSS by the hydrophilic head. Therefore, strong intermolecular interactions were created between PDMS and PEDOT:PSS [133]. The strong intermolecular force between polymer composite elements and the improvement of mechanical properties by PEG and Triton X-100 made the polymer composite durable. Therefore, the current did not reduce during 1000 opening/closing cycles, and it decreased  $\sim 2.7\%$  at the 5000<sup>th</sup> opening/closing cycle.

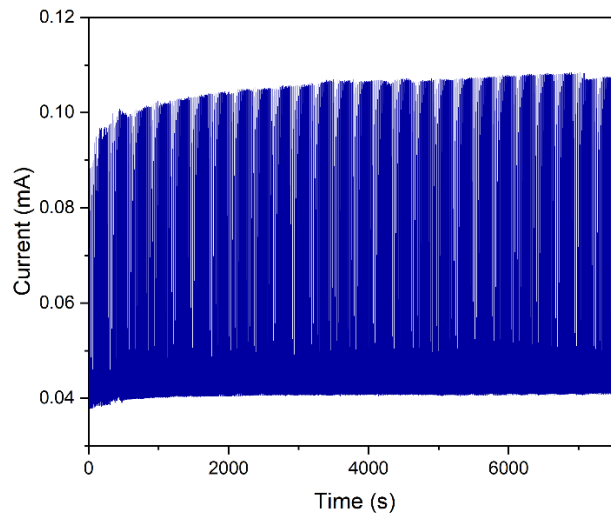


Figure 4.13 Current-time graphs for (a) complete period of 5000 opening/closing cycles, (b) initial, (c) 1000, and (d) 5000 opening/closing cycles for the kirigami structured polymer composite sample

## 4.4 Application

Kirigami structured PEDOT:PSS/PDMS polymer composites can be used as conductors in flexible and stretchable electronic devices due to their conductivity and reliability. In addition to their application as conductors for electronic devices, they can be used as strain sensors. A fundamental parameter in the strain sensors is their sensitivity to strain. The sensitivity was investigated by monitoring resistance changes during stretching using the gauge factor. The gauge factor is the ratio of relative change in electrical resistance to the relative change in length (strain) [153].

Figures 4.14a and 4.14b show the resistance changes correspond to stretching. The gauge factor increased linearly with strain from 0.33 to 1.72 for the kirigami structured polymer composite and from 0.6 to 1.3 for the kirigami structured PEDOT:PSS coated PDMS when the strain changed from 25% to 95%.

The resistance changes for stretching and strain release are shown in Figures 12c and 12d. The corresponding hysteresis is calculated by Eq. (6) [154].

$$h(\%) = \left| \frac{R_s - R_r}{R_m} \right| \times 100 \quad (4-6)$$

where “ $R_s$ ” and “ $R_r$ ” are resistance at stretching and releasing states, respectively and “ $R_m$ ” is the maximum value of resistance at specific strain. The relative resistance changes had negligible hysteresis ( $\sim 3.5\%$ ) for kirigami structured PEDOT:PSS coated PDMS and polymer composite samples.

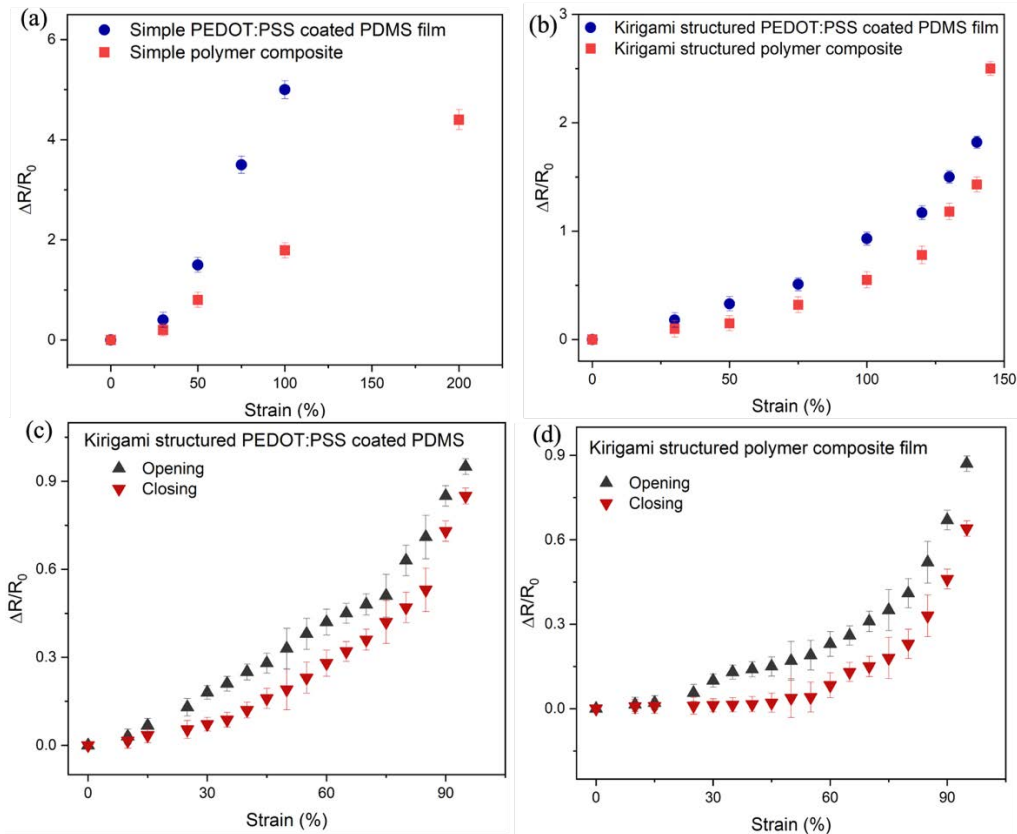


Figure 4.14  $\Delta R/R_0$  versus strain for (a) non-kirigami and (b) kirigami structured samples at different strains;  $\Delta R/R_0$  for opening and closing for (c) kirigami structured PEDOT:PSS coated PDMS and (d) kirigami structured polymer composite samples

To demonstrate the application of kirigami structured polymer composite for human body movement detection, we attached the specimen to a human wrist (Figure 4.15a). An electrical circuit based on the schematic shown in Figure 4.15b was used to record generated signals. As shown in Figure 4.15c, when the wrist was bent up or down, the kirigami structured sample

stretched and became in the open state and consequently, the resistance increased. In contrast, the resistance was constant when the rest was in a neutral position (the kirigami structured sample was in the closed state).

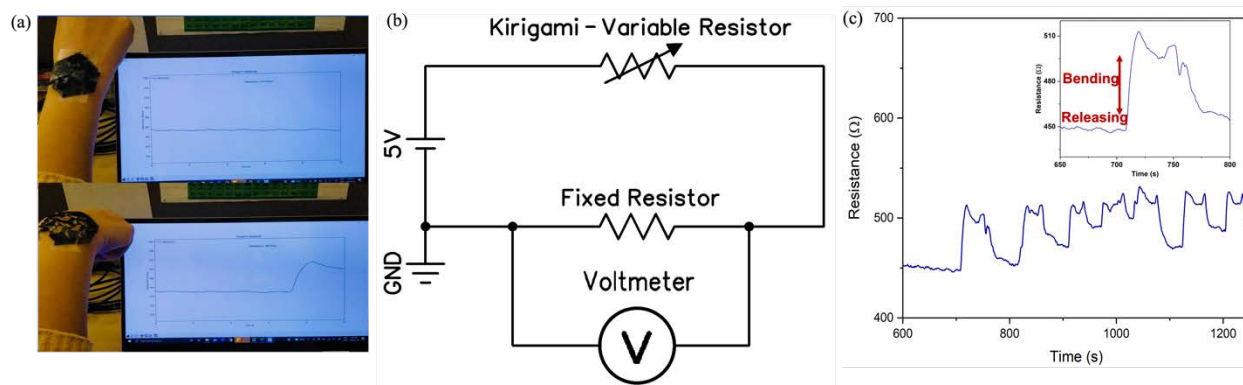


Figure 4.15 (a) Photographs of kirigami structured polymer composite attached to a human wrist, (b) the schematic of electrical circuit used for detecting signals generated by wrist bending, and (c) resistance variation by wrist bending

## CHAPTER 5 CONCLUSION AND RECOMMENDATIONS

Wearable electronics are one of the interesting new subjects in the electronics field, especially for health monitoring applications. Stretchability and durability are the main challenges in wearable electronics.

Kirigami patterns and mixing elastomeric polymers with conductive fillers are promising approaches to make electronic devices stretchable. In this project, these two methods were employed to increase the stretchability of conductors. For this purpose, PEDOT:PSS/PDMS polymer composite films were cut by a laser cutting technique to make kirigami structures. The auxetic, bistable and omnidirectional kirigami structure was designed by perforated parallel cuts on the films.

In this thesis, the tensile strength of non-kirigami and kirigami samples was examined. The results showed that the kirigami structured polymer composite had higher tensile strength than the kirigami structured PDMS and PEDOT:PSS coated PDMS. The elongation at break for the kirigami structured specimens increased compared to the non-kirigami samples. The elongation at break for non-kirigami samples had the same trend as the kirigami ones. The non-kirigami PEDOT:PSS coated PDMS had higher Young's modulus (2 MPa) than non-kirigami PDMS (0.75 MPa) and non-kirigami polymer composite samples (0.21 MPa). Therefore, it can be concluded PEDOT:PSS coating decreased stretchability.

The plastic deformation was zero for one loading/unloading cycle when different strains (25%, 35%, 45%, and 55%) were applied to the non-kirigami and kirigami structured specimens. However, they showed a small percentage of plastic deformation under 500 loading/unloading cycles at 25% strain. The plastic deformation of kirigami structured specimens was less than the plastic deformation of non-kirigami specimens. The Mullin's softening effect was observed in cyclic loading/unloading due to structural damages.

The hysteresis loop caused by loading/unloading samples represents their viscoelastic behavior. The viscoelastic behavior leads to energy dissipation during loading/unloading. Therefore, more energy dissipation shows more viscoelastic behavior. The energy dissipation is calculated from the area inside the hysteresis loop. Results showed that the energy dissipation of kirigami structured specimens is less than the energy dissipation of non-kirigami samples. These results confirmed that

the behavior of kirigami structured is closed to spring-like behavior (elastic behavior). In addition, the kirigami structured polymer composite samples had less energy dissipation ( $\sim 0.3$  J) than other samples.

A dynamic mechanical test was performed by applying a sinusoidal strain with 25% amplitude to calculate complex modulus, elastic modulus, storage modulus, angular phase difference and loss factor. These results also confirmed that elasticity increased in the kirigami structured specimens.

The electromechanical responses of non-kirigami and kirigami structured samples were investigated at different strains. For all samples, the current decreased by increasing strain. Results showed that the stretchability increased in the kirigami structured samples, and they showed less current reduction compared to the non-kirigami samples.

The electromechanical responses of non-kirigami and kirigami samples were studied when the samples were exposed to 25% strain under 1000 and 5000 loading/unloading cycles, respectively. The electromechanical response of kirigami structured polymer composite and PEDOT:PSS coated PDMS samples reduced 2.7% and 56%, respectively. The results showed that kirigami patterns affect the stability of electromechanical responses. The kirigami structured polymer composite showed current stability and durability under many opening/closing cycles (i.e., 5000 cycles). However, the current response of the kirigami structured PEDOT:PSS coated PDMS sample was detrimental for 5000 opening/closing cycles. Cracks and wrinkles generated by the applied strain led to the change in the current amplitude of all specimens.

The application of kirigami structured polymer composite was evaluated for human motion detection. It showed our work paves the way to develop future stretchable and deformable strain sensors based on kirigami-inspired conducting polymers. The sensitivity of kirigami structured samples was characterized by a gauge factor. In addition, the hysteresis of electrical resistance was studied. Both kirigami structured specimens showed approximately the same gauge factor ( $\sim 0.5$  to 1.5) and hysteresis of electrical resistance ( $\sim 3.5\%$ ).



## 5.1 Recommendations

In this Thesis, we showed the application of kirigami structured polymer composite as a strain sensor for human body movement detection. However, further research such as the following can be done:

- Examining the fatigue resistance of samples: Fatigue resistance is the maximum value of stress that samples can resist under a certain number of loading/unloading cycles without failure.
- In this thesis, the application of kirigami structures as a sensor for body movement detection was evaluated. It is suggested to assess the skin compatibility of the sensor too.
- Evaluating sensitivity of kirigami structured polymer composite in other parts of the body such as the face, fingers, and knee.

Also, for further work, the following suggestions are recommended:

- Using other kinds of elastomeric polymers such as polyurethane and conductive filler such as metal nanowires, CNT, etc.
- Investigating the stretchability and durability of other kirigami structured geometries
- Manipulating both origami and kirigami concepts for improving stretchability and stability
- Using biocompatible and biodegradable polymers such as polylactic acid to make a skin-compatible sensor for health monitoring

## REFERENCES

- [1] T. Nezakati, A. Seifalian, A. Tan, and A. M. Seifalian, “Conductive Polymers: Opportunities and Challenges in Biomedical Applications,” *Chemical Reviews*, vol. 118, no. 14, pp. 6766–6843, Jul. 2018, doi: 10.1021/acs.chemrev.6b00275.
- [2] S. Nagels and W. Deferme, “Fabrication Approaches to Interconnect Based Devices for Stretchable Electronics: A Review,” *Materials*, vol. 11, no. 3, Mar. 2018, doi: 10.3390/ma11030375.
- [3] L. Groenendaal, F. Jonas, D. Freitag, H. Pielartzik, and J. R. Reynolds, “Poly(3,4-ethylenedioxythiophene) and Its Derivatives: Past, Present, and Future,” *Advanced Materials*, vol. 12, no. 7, Apr. 2000, doi: 10.1002/(SICI)1521-4095(200004)12:7<481::AID-ADMA481>3.0.CO;2-C.
- [4] W. Wu, “Stretchable electronics: functional materials, fabrication strategies and applications,” *Science and Technology of Advanced Materials*, vol. 20, no. 1, Dec. 2019, doi: 10.1080/14686996.2018.1549460.
- [5] Y. Qian *et al.*, “Stretchable Organic Semiconductor Devices,” *Advanced Materials*, vol. 28, no. 42, Nov. 2016, doi: 10.1002/adma.201601278.
- [6] S. Peng, Y. Yu, S. Wu, and C.-H. Wang, “Conductive Polymer Nanocomposites for Stretchable Electronics: Material Selection, Design, and Applications,” *ACS Applied Materials & Interfaces*, vol. 13, no. 37, pp. 43831–43854, Sep. 2021, doi: 10.1021/acsami.1c15014.
- [7] D.-H. Kim *et al.*, “Stretchable and Foldable Silicon Integrated Circuits,” *Science (1979)*, vol. 320, no. 5875, Apr. 2008, doi: 10.1126/science.1154367.

- [8] J. A. Rogers, T. Someya, and Y. Huang, “Materials and Mechanics for Stretchable Electronics,” *Science (1979)*, vol. 327, no. 5973, Mar. 2010, doi: 10.1126/science.1182383.
- [9] S. Yoon *et al.*, “Highly stretchable metal-polymer hybrid conductors for wearable and self-cleaning sensors,” *NPG Asia Materials*, vol. 13, no. 1, p. 4, Dec. 2021, doi: 10.1038/s41427-020-00277-6.
- [10] Z. Yu, X. Niu, Z. Liu, and Q. Pei, “Intrinsically Stretchable Polymer Light-Emitting Devices Using Carbon Nanotube-Polymer Composite Electrodes,” *Advanced Materials*, vol. 23, no. 34, pp. 3989–3994, Sep. 2011, doi: 10.1002/adma.201101986.
- [11] Y. Kim *et al.*, “Stretchable nanoparticle conductors with self-organized conductive pathways,” *Nature*, vol. 500, no. 7460, pp. 59–63, Aug. 2013, doi: 10.1038/nature12401.
- [12] D. Corzo, G. Tostado-Blázquez, and D. Baran, “Flexible Electronics: Status, Challenges and Opportunities,” *Frontiers in Electronics*, vol. 1, Sep. 2020, doi: 10.3389/felec.2020.594003.
- [13] A. Polywka, T. Jakob, L. Stegers, T. Riedl, and P. Görrn, “Facile Preparation of High-Performance Elastically Stretchable Interconnects,” *Advanced Materials*, vol. 27, no. 25, pp. 3755–3759, Jul. 2015, doi: 10.1002/adma.201501461.
- [14] W. Dang, V. Vinciguerra, L. Lorenzelli, and R. Dahiya, “Printable stretchable interconnects,” *Flexible and Printed Electronics*, vol. 2, no. 1, p. 013003, Mar. 2017, doi: 10.1088/2058-8585/aa5ab2.
- [15] J.-H. Ahn and J. H. Je, “Stretchable electronics: materials, architectures and integrations,” *Journal of Physics D: Applied Physics*, vol. 45, no. 10, Mar. 2012, doi: 10.1088/0022-3727/45/10/103001.
- [16] J.-Y. Hong, W. Kim, D. Choi, J. Kong, and H. S. Park, “Omnidirectionally Stretchable and Transparent Graphene Electrodes,” *ACS Nano*, vol. 10, no. 10, pp. 9446–9455, Oct. 2016, doi: 10.1021/acsnano.6b04493.
- [17] Y. Zhang *et al.*, “Printing, folding and assembly methods for forming 3D mesostructures in advanced materials,” *Nature Reviews Materials*, vol. 2, no. 4, Apr. 2017, doi: 10.1038/natrevmats.2017.19.

- [18] X. Cheng and Y. Zhang, “Micro/Nanoscale 3D Assembly by Rolling, Folding, Curving, and Buckling Approaches,” *Advanced Materials*, vol. 31, no. 36, Sep. 2019, doi: 10.1002/adma.201901895.
- [19] S. Chen, J. Chen, X. Zhang, Z.-Y. Li, and J. Li, “Kirigami/origami: unfolding the new regime of advanced 3D microfabrication/nanofabrication with ‘folding,’” *Light: Science & Applications*, vol. 9, no. 1, Dec. 2020, doi: 10.1038/s41377-020-0309-9.
- [20] C. Park, J. Yoon, and E. L. Thomas, “Enabling nanotechnology with self assembled block copolymer patterns,” *Polymer (Guildf)*, vol. 44, no. 22, pp. 6725–6760, Oct. 2003, doi: 10.1016/j.polymer.2003.08.011.
- [21] A. Biswas, I. S. Bayer, A. S. Biris, T. Wang, E. Dervishi, and F. Faupel, “Advances in top–down and bottom–up surface nanofabrication: Techniques, applications & future prospects,” *Advances in Colloid and Interface Science*, vol. 170, no. 1–2, Jan. 2012, doi: 10.1016/j.cis.2011.11.001.
- [22] S. Kumar, P. Bhushan, and S. Bhattacharya, “Fabrication of Nanostructures with Bottom-up Approach and Their Utility in Diagnostics, Therapeutics, and Others,” 2018. doi: 10.1007/978-981-10-7751-7\_8.
- [23] Y. Zhang *et al.*, “Printing, folding and assembly methods for forming 3D mesostructures in advanced materials,” *Nature Reviews Materials*, vol. 2, no. 4, p. 17019, Apr. 2017, doi: 10.1038/natrevmats.2017.19.
- [24] K. Gregorczyk and M. Knez, “Hybrid nanomaterials through molecular and atomic layer deposition: Top down, bottom up, and in-between approaches to new materials,” *Progress in Materials Science*, vol. 75, pp. 1–37, Jan. 2016, doi: 10.1016/j.pmatsci.2015.06.004.
- [25] Y. Zhao, S. He, M. Wei, D. G. Evans, and X. Duan, “Hierarchical films of layered double hydroxides by using a sol–gel process and their high adaptability in water treatment,” *Chemical Communications*, vol. 46, no. 17, p. 3031, 2010, doi: 10.1039/b926906a.

- [26] J. C. Huie, “Guided molecular self-assembly: a review of recent efforts,” *Smart Materials and Structures*, vol. 12, no. 2, pp. 264–271, Apr. 2003, doi: 10.1088/0964-1726/12/2/315.
- [27] A. R. Biris *et al.*, “High-Quality Double-Walled Carbon Nanotubes Grown by a Cold-Walled Radio Frequency Chemical Vapor Deposition Process,” *Chemistry of Materials*, vol. 20, no. 10, pp. 3466–3472, May 2008, doi: 10.1021/cm703680n.
- [28] H. Zhao *et al.*, “Nanofabrication approaches for functional three-dimensional architectures,” *Nano Today*, vol. 30, Feb. 2020, doi: 10.1016/j.nantod.2019.100825.
- [29] T. J. Cui, D. R. Smith, and R. Liu, Eds., *Metamaterials*. Boston: Springer, 2010. Accessed: Sep. 15, 2021. [Online]. Available: <https://link.springer.com/content/pdf/10.1007/978-1-4419-0573-4.pdf>
- [30] R. M. Neville, F. Scarpa, and A. Pirrera, “Shape morphing Kirigami mechanical metamaterials,” *Scientific Reports*, vol. 6, no. 1, Nov. 2016, doi: 10.1038/srep31067.
- [31] J. J. Park, P. Won, and S. H. Ko, “A Review on Hierarchical Origami and Kirigami Structure for Engineering Applications,” *International Journal of Precision Engineering and Manufacturing-Green Technology*, vol. 6, no. 1, Jan. 2019, doi: 10.1007/s40684-019-00027-2.
- [32] K. Cai, J. Luo, Y. Ling, J. Wan, and Q. Qin, “Effects of size and surface on the auxetic behaviour of monolayer graphene kirigami,” *Scientific Reports*, vol. 6, no. 1, Dec. 2016, doi: 10.1038/srep35157.
- [33] Y. Yang, M. A. Dias, and D. P. Holmes, “Multistable kirigami for tunable architected materials,” *Physical Review Materials*, vol. 2, no. 11, Nov. 2018, doi: 10.1103/PhysRevMaterials.2.110601.
- [34] N. Yang, M. Zhang, and R. Zhu, “3D kirigami metamaterials with coded thermal expansion properties,” *Extreme Mech Lett*, vol. 40, Oct. 2020, doi: 10.1016/j.eml.2020.100912.

- [35] Y. Tang and J. Yin, "Design of cut unit geometry in hierarchical kirigami-based auxetic metamaterials for high stretchability and compressibility," *Extreme Mech Lett*, vol. 12, pp. 77–85, Apr. 2017, doi: 10.1016/j.eml.2016.07.005.
- [36] W. Wang *et al.*, "Controlling the laser induction and cutting process on polyimide films for kirigami-inspired supercapacitor applications," *Science China Technological Sciences*, vol. 64, no. 3, Mar. 2021, doi: 10.1007/s11431-019-1543-y.
- [37] Y. Guo *et al.*, "Additive manufacturing of patterned 2D semiconductor through recyclable masked growth," *Proceedings of the National Academy of Sciences*, vol. 116, no. 9, Feb. 2019, doi: 10.1073/pnas.1816197116.
- [38] S. Xu *et al.*, "Assembly of micro/nanomaterials into complex, three-dimensional architectures by compressive buckling," *Science (1979)*, vol. 347, no. 6218, Jan. 2015, doi: 10.1126/science.1260960.
- [39] X. Zhou *et al.*, "All 3D-printed stretchable piezoelectric nanogenerator with non-protruding kirigami structure," *Nano Energy*, vol. 72, Jun. 2020, doi: 10.1016/j.nanoen.2020.104676.
- [40] D. J. Lipomi *et al.*, "Skin-like pressure and strain sensors based on transparent elastic films of carbon nanotubes," *Nature Nanotechnology*, vol. 6, no. 12, Dec. 2011, doi: 10.1038/nnano.2011.184.
- [41] J. Lyu *et al.*, "Stretchable conductors by kirigami patterning of aramid-silver nanocomposites with zero conductance gradient," *Applied Physics Letters*, vol. 111, no. 16, p. 161901, Oct. 2017, doi: 10.1063/1.5001094.
- [42] Z. Wang, L. Zhang, S. Duan, H. Jiang, J. Shen, and C. Li, "Kirigami-patterned highly stretchable conductors from flexible carbon nanotube-embedded polymer films," *J. Mater. Chem. C*, vol. 5, no. 34, pp. 8714–8722, 2017, doi: 10.1039/C7TC01727H.
- [43] Y. Guan, Z. Zhang, Y. Tang, J. Yin, and S. Ren, "Kirigami-Inspired Nanoconfined Polymer Conducting Nanosheets with 2000% Stretchability," *Advanced Materials*, vol. 30, no. 20, May 2018, doi: 10.1002/adma.201706390.
- [44] Y. Kim, O. Y. Kweon, Y. Won, and J. H. Oh, "Deformable and Stretchable Electrodes for Soft Electronic Devices," *Macromolecular Research*, vol. 27, no. 7, Jul. 2019, doi: 10.1007/s13233-019-7175-4.

- [45] S. Huang, Y. Liu, Y. Zhao, Z. Ren, and C. F. Guo, "Flexible Electronics: Stretchable Electrodes and Their Future," *Advanced Functional Materials*, vol. 29, no. 6, Feb. 2019, doi: 10.1002/adfm.201805924.
- [46] J. Liang *et al.*, "Silver Nanowire Percolation Network Soldered with Graphene Oxide at Room Temperature and Its Application for Fully Stretchable Polymer Light-Emitting Diodes," *ACS Nano*, vol. 8, no. 2, pp. 1590–1600, Feb. 2014, doi: 10.1021/nn405887k.
- [47] M. Y. Lee *et al.*, "Highly Flexible Organic Nanofiber Phototransistors Fabricated on a Textile Composite for Wearable Photosensors," *Advanced Functional Materials*, vol. 26, no. 9, pp. 1445–1453, Mar. 2016, doi: 10.1002/adfm.201503230.
- [48] J. H. Song *et al.*, "Surface-Embedded Stretchable Electrodes by Direct Printing and their Uses to Fabricate Ultrathin Vibration Sensors and Circuits for 3D Structures," *Advanced Materials*, vol. 29, no. 43, Nov. 2017, doi: 10.1002/adma.201702625.
- [49] C.-H. Jun, S. Ohisa, Y.-J. Pu, T. Chiba, and J. Kido, "Comparison of Spin and Blade Coating Methods in Solution-process for Organic Light-emitting Devices," *Journal of Photopolymer Science and Technology*, vol. 28, no. 3, pp. 343–347, 2015, doi: 10.2494/photopolymer.28.343.
- [50] M. Shin, J. H. Song, G.-H. Lim, B. Lim, J.-J. Park, and U. Jeong, "Highly Stretchable Polymer Transistors Consisting Entirely of Stretchable Device Components," *Advanced Materials*, vol. 26, no. 22, Jun. 2014, doi: 10.1002/adma.201400009.
- [51] D. Stauffer and A. Aharony, *Introduction To Percolation Theory*. Taylor & Francis, 2018. doi: 10.1201/9781315274386.
- [52] R. Ram, M. Rahaman, A. Aldalbahi, and D. Khastgir, "Determination of percolation threshold and electrical conductivity of polyvinylidene fluoride (PVDF)/short carbon fiber (SCF) composites: effect of SCF aspect ratio," *Polymer International*, vol. 66, no. 4, Apr. 2017, doi: 10.1002/pi.5294.
- [53] P. Lee *et al.*, "Highly Stretchable and Highly Conductive Metal Electrode by Very Long Metal Nanowire Percolation Network," *Advanced Materials*, vol. 24, no. 25, Jul. 2012, doi: 10.1002/adma.201200359.

- [54] H.-J. Choi, M. S. Kim, D. Ahn, S. Y. Yeo, and S. Lee, “Electrical percolation threshold of carbon black in a polymer matrix and its application to antistatic fibre,” *Scientific Reports*, vol. 9, no. 1, Dec. 2019, doi: 10.1038/s41598-019-42495-1.
- [55] T. Sekitani, Y. Noguchi, K. Hata, T. Fukushima, T. Aida, and T. Someya, “A Rubberlike Stretchable Active Matrix Using Elastic Conductors,” *Science (1979)*, vol. 321, no. 5895, pp. 1468–1472, Sep. 2008, doi: 10.1126/science.1160309.
- [56] Y. Zhang *et al.*, “Polymer-Embedded Carbon Nanotube Ribbons for Stretchable Conductors,” *Advanced Materials*, vol. 22, no. 28, Jun. 2010, doi: 10.1002/adma.200904426.
- [57] Y.-L. Li, I. A. Kinloch, and A. H. Windle, “Direct Spinning of Carbon Nanotube Fibers from Chemical Vapor Deposition Synthesis,” *Science (1979)*, vol. 304, no. 5668, pp. 276–278, Apr. 2004, doi: 10.1126/science.1094982.
- [58] K. Jiang, Q. Li, and S. Fan, “Spinning continuous carbon nanotube yarns,” *Nature*, vol. 419, no. 6909, pp. 801–801, Oct. 2002, doi: 10.1038/419801a.
- [59] Y. Shang *et al.*, “Super-Stretchable Spring-Like Carbon Nanotube Ropes,” *Advanced Materials*, vol. 24, no. 21, pp. 2896–2900, Jun. 2012, doi: 10.1002/adma.201200576.
- [60] B.-W. Wang *et al.*, “Continuous Fabrication of Meter-Scale Single-Wall Carbon Nanotube Films and their Use in Flexible and Transparent Integrated Circuits,” *Advanced Materials*, vol. 30, no. 32, p. 1802057, Aug. 2018, doi: 10.1002/adma.201802057.
- [61] D. J. Lipomi *et al.*, “Skin-like pressure and strain sensors based on transparent elastic films of carbon nanotubes,” *Nature Nanotechnology*, vol. 6, no. 12, pp. 788–792, Dec. 2011, doi: 10.1038/nnano.2011.184.
- [62] H.-Z. Geng, K. K. Kim, K. P. So, Y. S. Lee, Y. Chang, and Y. H. Lee, “Effect of Acid Treatment on Carbon Nanotube-Based Flexible Transparent Conducting Films,” *J Am Chem Soc*, vol. 129, no. 25, pp. 7758–7759, Jun. 2007, doi: 10.1021/ja0722224.
- [63] H.-S. Kim *et al.*, “Lead Iodide Perovskite Sensitized All-Solid-State Submicron Thin Film Mesoscopic Solar Cell with Efficiency Exceeding 9%,” *Scientific Reports*, vol. 2, no. 1, p. 591, Dec. 2012, doi: 10.1038/srep00591.



- [64] Y. Zhao, A. Kim, G. Wan, and B. C. K. Tee, "Design and applications of stretchable and self-healable conductors for soft electronics," *Nano Convergence*, vol. 6, no. 1, p. 25, Dec. 2019, doi: 10.1186/s40580-019-0195-0.
- [65] N. K. Unsworth *et al.*, "Comparison of dimethyl sulfoxide treated highly conductive poly(3,4-ethylenedioxythiophene):poly(styrenesulfonate) electrodes for use in indium tin oxide-free organic electronic photovoltaic devices," *Organic Electronics*, vol. 15, no. 10, Oct. 2014, doi: 10.1016/j.orgel.2014.07.015.
- [66] Y. Wang *et al.*, "A highly stretchable, transparent, and conductive polymer," *Science Advances*, vol. 3, no. 3, Mar. 2017, doi: 10.1126/sciadv.1602076.
- [67] M. Vosgueritchian, D. J. Lipomi, and Z. Bao, "Highly Conductive and Transparent PEDOT:PSS Films with a Fluorosurfactant for Stretchable and Flexible Transparent Electrodes," *Advanced Functional Materials*, vol. 22, no. 2, Jan. 2012, doi: 10.1002/adfm.201101775.
- [68] P. A. Levermore, L. Chen, X. Wang, R. Das, and D. D. C. Bradley, "Fabrication of Highly Conductive Poly(3,4-ethylenedioxythiophene) Films by Vapor Phase Polymerization and Their Application in Efficient Organic Light-Emitting Diodes," *Advanced Materials*, vol. 19, no. 17, Sep. 2007, doi: 10.1002/adma.200700614.
- [69] T. F. O'Connor *et al.*, "Wearable organic solar cells with high cyclic bending stability: Materials selection criteria," *Solar Energy Materials and Solar Cells*, vol. 144, Jan. 2016, doi: 10.1016/j.solmat.2015.09.049.
- [70] M.-W. Lee, M.-Y. Lee, J.-C. Choi, J.-S. Park, and C.-K. Song, "Fine patterning of glycerol-doped PEDOT:PSS on hydrophobic PVP dielectric with ink jet for source and drain electrode of OTFTs," *Organic Electronics*, vol. 11, no. 5, May 2010, doi: 10.1016/j.orgel.2010.01.028.
- [71] Z. Li *et al.*, "Free-Standing Conducting Polymer Films for High-Performance Energy Devices," *Angewandte Chemie International Edition*, vol. 55, no. 3, Jan. 2016, doi: 10.1002/anie.201509033.

- [72] L. v. Kayser and D. J. Lipomi, “Stretchable Conductive Polymers and Composites Based on PEDOT and PEDOT:PSS,” *Advanced Materials*, vol. 31, no. 10, Mar. 2019, doi: 10.1002/adma.201806133.
- [73] Y. Zhu and F. Xu, “Buckling of Aligned Carbon Nanotubes as Stretchable Conductors: A New Manufacturing Strategy,” *Advanced Materials*, vol. 24, no. 8, pp. 1073–1077, Feb. 2012, doi: 10.1002/adma.201103382.
- [74] J. Zhang and E. P. Fahrenthold, “Conductance of Buckled  $N = 5$  Armchair Graphene Nanoribbons,” *The Journal of Physical Chemistry Letters*, vol. 11, no. 4, pp. 1378–1383, Feb. 2020, doi: 10.1021/acs.jpcclett.0c00047.
- [75] Y. Zhang *et al.*, “Experimental and Theoretical Studies of Serpentine Microstructures Bonded To Prestrained Elastomers for Stretchable Electronics,” *Advanced Functional Materials*, vol. 24, no. 14, pp. 2028–2037, Apr. 2014, doi: 10.1002/adfm.201302957.
- [76] D. Brosteaux, Fabrice Axisa, M. Gonzalez, and J. Vanfleteren, “Design and Fabrication of Elastic Interconnections for Stretchable Electronic Circuits,” *IEEE Electron Device Letters*, vol. 28, no. 7, pp. 552–554, Jul. 2007, doi: 10.1109/LED.2007.897887.
- [77] C. F. Guo, T. Sun, Q. Liu, Z. Suo, and Z. Ren, “Highly stretchable and transparent nanomesh electrodes made by grain boundary lithography,” *Nature Communications*, vol. 5, no. 1, p. 3121, May 2014, doi: 10.1038/ncomms4121.
- [78] X. Hu, Y. Dou, J. Li, and Z. Liu, “Buckled Structures: Fabrication and Applications in Wearable Electronics,” *Small*, vol. 15, no. 32, p. 1804805, Aug. 2019, doi: 10.1002/smll.201804805.
- [79] C. Lv, H. Yu, and H. Jiang, “Archimedean spiral design for extremely stretchable interconnects,” *Extreme Mech Lett*, vol. 1, pp. 29–34, Dec. 2014, doi: 10.1016/j.eml.2014.12.008.
- [80] A. Mamidanna, Z. Song, C. Lv, C. S. Lefky, H. Jiang, and O. J. Hildreth, “Printing Stretchable Spiral Interconnects Using Reactive Ink Chemistries,” *ACS Applied Materials & Interfaces*, vol. 8, no. 20, pp. 12594–12598, May 2016, doi: 10.1021/acsami.6b03922.

- [81] Y. Zhang *et al.*, “Mechanics of ultra-stretchable self-similar serpentine interconnects,” *Acta Materialia*, vol. 61, no. 20, pp. 7816–7827, Dec. 2013, doi: 10.1016/j.actamat.2013.09.020.
- [82] C. Chen, S. Chen, W. Gu, H. Zhang, and B. Liu, “Characterization of delamination failure of two-dimensional horseshoe stretchable interconnects using digital image correlation,” *Polymer Testing*, vol. 94, p. 107041, Feb. 2021, doi: 10.1016/j.polymertesting.2020.107041.
- [83] T. Cheng, Y. Zhang, W.-Y. Lai, and W. Huang, “Stretchable Thin-Film Electrodes for Flexible Electronics with High Deformability and Stretchability,” *Advanced Materials*, vol. 27, no. 22, pp. 3349–3376, Jun. 2015, doi: 10.1002/adma.201405864.
- [84] J. A. Fan *et al.*, “Fractal design concepts for stretchable electronics,” *Nature Communications*, vol. 5, no. 1, May 2014, doi: 10.1038/ncomms4266.
- [85] Y. Won, A. Kim, W. Yang, S. Jeong, and J. Moon, “A highly stretchable, helical copper nanowire conductor exhibiting a stretchability of 700%,” *NPG Asia Materials*, vol. 6, no. 9, pp. e132–e132, Sep. 2014, doi: 10.1038/am.2014.88.
- [86] X. Xu *et al.*, “Three-dimensional helical inorganic thermoelectric generators and photodetectors for stretchable and wearable electronic devices,” *Journal of Materials Chemistry C*, vol. 6, no. 18, pp. 4866–4872, 2018, doi: 10.1039/C8TC01183D.
- [87] Y. Shang *et al.*, “Self-stretchable, helical carbon nanotube yarn supercapacitors with stable performance under extreme deformation conditions,” *Nano Energy*, vol. 12, pp. 401–409, Mar. 2015, doi: 10.1016/j.nanoen.2014.11.048.
- [88] J. Yu *et al.*, “A High Performance Stretchable Asymmetric Fiber-Shaped Supercapacitor with a Core-Sheath Helical Structure,” *Advanced Energy Materials*, vol. 7, no. 3, p. 1600976, Feb. 2017, doi: 10.1002/aenm.201600976.
- [89] K.-I. Jang *et al.*, “Self-assembled three dimensional network designs for soft electronics,” *Nature Communications*, vol. 8, no. 1, p. 15894, Aug. 2017, doi: 10.1038/ncomms15894.

- [90] D.-H. Kim *et al.*, “Materials and noncoplanar mesh designs for integrated circuits with linear elastic responses to extreme mechanical deformations,” *Proceedings of the National Academy of Sciences*, vol. 105, no. 48, pp. 18675–18680, Dec. 2008, doi: 10.1073/pnas.0807476105.
- [91] R. Guo *et al.*, “Biomimicking Topographic Elastomeric Petals (E-Petals) for Omnidirectional Stretchable and Printable Electronics,” *Advanced Science*, vol. 2, no. 3, p. 1400021, Mar. 2015, doi: 10.1002/advs.201400021.
- [92] H.-B. Lee *et al.*, “Mogul-Patterned Elastomeric Substrate for Stretchable Electronics,” *Advanced Materials*, vol. 28, no. 16, pp. 3069–3077, Apr. 2016, doi: 10.1002/adma.201505218.
- [93] L. Xu, T. C. Shyu, and N. A. Kotov, “Origami and Kirigami Nanocomposites,” *ACS Nano*, vol. 11, no. 8, pp. 7587–7599, Aug. 2017, doi: 10.1021/acsnano.7b03287.
- [94] Y. Chen, J. Yan, and J. Feng, “Geometric and Kinematic Analyses and Novel Characteristics of Origami-Inspired Structures,” *Symmetry (Basel)*, vol. 11, no. 9, p. 1101, Sep. 2019, doi: 10.3390/sym11091101.
- [95] Z. Song, “Studies of origami and kirigami and their applications,” Arizona State University, 2016.
- [96] M. Johnson *et al.*, “Fabricating biomedical origami: a state-of-the-art review,” *International Journal of Computer Assisted Radiology and Surgery*, vol. 12, no. 11, Nov. 2017, doi: 10.1007/s11548-017-1545-1.
- [97] A. Taylor, M. Miller, M. Fok, K. Nilsson, and Z. Tsz Ho Tse, “Intracardiac Magnetic Resonance Imaging Catheter With Origami Deployable Mechanisms1,” *Journal of Medical Devices*, vol. 10, no. 2, Jun. 2016, doi: 10.1115/1.4033151.
- [98] S. Zhu and T. Li, “Hydrogenation-Assisted Graphene Origami and Its Application in Programmable Molecular Mass Uptake, Storage, and Release,” *ACS Nano*, vol. 8, no. 3, Mar. 2014, doi: 10.1021/nm500025t.
- [99] J. C. Breger *et al.*, “Self-Folding Thermo-Magnetically Responsive Soft Microgrippers,” *ACS Applied Materials & Interfaces*, vol. 7, no. 5, pp. 3398–3405, Feb. 2015, doi: 10.1021/am508621s.

- [100] D. Grimm *et al.*, “Rolled-up nanomembranes as compact 3D architectures for field effect transistors and fluidic sensing applications,” *Nano Letters*, vol. 13, no. 1, pp. 213–218, Jan. 2013, doi: 10.1021/nl303887b.
- [101] Y. Li, W. Liu, Y. Deng, W. Hong, and H. Yu, “Miura-ori enabled stretchable circuit boards,” *npj Flexible Electronics*, vol. 5, no. 1, Dec. 2021, doi: 10.1038/s41528-021-00099-8.
- [102] B. Grünbaum and G. C. Shephard, *Tilings and patterns*. 1987.
- [103] A. Rafsanjani and D. Pasini, “Bistable auxetic mechanical metamaterials inspired by ancient geometric motifs,” *Extreme Mech Lett*, vol. 9, pp. 291–296, Dec. 2016, doi: 10.1016/j.eml.2016.09.001.
- [104] M. Isobe and K. Okumura, “Initial rigid response and softening transition of highly stretchable kirigami sheet materials,” *Scientific Reports*, vol. 6, no. 1, p. 24758, Apr. 2016, doi: 10.1038/srep24758.
- [105] G. P. T. Choi, L. H. Dudte, and L. Mahadevan, “Programming shape using kirigami tessellations,” *Nature Materials*, vol. 18, no. 9, pp. 999–1004, Sep. 2019, doi: 10.1038/s41563-019-0452-y.
- [106] A. Rafsanjani and K. Bertoldi, “Buckling-Induced Kirigami,” *Physical Review Letters*, vol. 118, no. 8, p. 084301, Feb. 2017, doi: 10.1103/PhysRevLett.118.084301.
- [107] L. Jin, A. E. Forte, B. Deng, A. Rafsanjani, and K. Bertoldi, “Kirigami-Inspired Inflatables with Programmable Shapes,” *Advanced Materials*, vol. 32, no. 33, p. 2001863, Aug. 2020, doi: 10.1002/adma.202001863.
- [108] Y. Zhang *et al.*, “A mechanically driven form of Kirigami as a route to 3D mesostructures in micro/nanomembranes,” *Proceedings of the National Academy of Sciences*, vol. 112, no. 38, pp. 11757–11764, Sep. 2015, doi: 10.1073/pnas.1515602112.
- [109] X. Shang, L. Liu, A. Rafsanjani, and D. Pasini, “Durable bistable auxetics made of rigid solids,” *Journal of Materials Research*, vol. 33, no. 3, pp. 300–308, Feb. 2018, doi: 10.1557/jmr.2017.417.

- [110] A. Salim, A. H. Naqvi, E. Park, A. D. Pham, and S. Lim, “Inkjet printed kirigami inspired split ring resonator for disposable, low cost strain sensor applications,” *Smart Materials and Structures*, vol. 29, no. 1, p. 015016, Jan. 2020, doi: 10.1088/1361-665X/ab548b.
- [111] D. S. Kong, J. Y. Han, Y. J. Ko, S. H. Park, M. Lee, and J. H. Jung, “A Highly Efficient and Durable Kirigami Triboelectric Nanogenerator for Rotational Energy Harvesting,” *Energies (Basel)*, vol. 14, no. 4, p. 1120, Feb. 2021, doi: 10.3390/en14041120.
- [112] X. Gong, Q. Yang, C. Zhi, and P. S. Lee, “Stretchable Energy Storage Devices: From Materials and Structural Design to Device Assembly,” *Advanced Energy Materials*, vol. 11, no. 15, p. 2003308, Apr. 2021, doi: 10.1002/aenm.202003308.
- [113] G. Li *et al.*, “PEDOT:PSS/Grafted-PDMS Electrodes for Fully Organic and Intrinsically Stretchable Skin-like Electronics,” *ACS Applied Materials & Interfaces*, vol. 11, no. 10, Mar. 2019, doi: 10.1021/acsami.8b20255.
- [114] K. Xu, Y. Lu, S. Honda, T. Arie, S. Akita, and K. Takei, “Highly stable kirigami-structured stretchable strain sensors for perdurable wearable electronics,” *Journal of Materials Chemistry C*, vol. 7, no. 31, pp. 9609–9617, 2019, doi: 10.1039/C9TC01874C.
- [115] T. H. Yang, H. Hida, D. Ichige, J. Mizuno, C. Robert Kao, and J. Shintake, “Foldable Kirigami Paper Electronics,” *physica status solidi (a)*, vol. 217, no. 9, p. 1900891, May 2020, doi: 10.1002/pssa.201900891.
- [116] P. Won *et al.*, “Stretchable and Transparent Kirigami Conductor of Nanowire Percolation Network for Electronic Skin Applications,” *Nano Letters*, vol. 19, no. 9, pp. 6087–6096, Sep. 2019, doi: 10.1021/acs.nanolett.9b02014.
- [117] Y. Diao *et al.*, “Kirigami electrodes of conducting polymer nanofibers for wearable humidity dosimeters and stretchable supercapacitors,” *Journal of Materials Chemistry A*, vol. 9, no. 15, pp. 9849–9857, 2021, doi: 10.1039/D0TA11335B.

- [118] Y. Kumaresan, G. Min, A. S. Dahiya, A. Ejaz, D. Shakthivel, and R. Dahiya, “Kirigami and Mogul-Patterned Ultra-Stretchable High-Performance ZnO Nanowires-Based Photodetector,” *Advanced Materials Technologies*, vol. 7, no. 1, p. 2100804, Jan. 2022, doi: 10.1002/admt.202100804.
- [119] J. Kim, H. Park, and S.-H. Jeong, “A kirigami concept for transparent and stretchable nanofiber networks-based conductors and UV photodetectors,” *Journal of Industrial and Engineering Chemistry*, vol. 82, pp. 144–152, Feb. 2020, doi: 10.1016/j.jiec.2019.10.006.
- [120] J.-H. Song, H.-J. Kim, M.-S. Kim, S.-H. Min, Y. Wang, and S.-H. Ahn, “Direct printing of performance tunable strain sensor via nanoparticle laser patterning process,” *Virtual and Physical Prototyping*, vol. 15, no. 3, pp. 265–277, Jul. 2020, doi: 10.1080/17452759.2020.1733431.
- [121] R. Sun *et al.*, “Kirigami stretchable strain sensors with enhanced piezoelectricity induced by topological electrodes,” *Applied Physics Letters*, vol. 112, no. 25, p. 251904, Jun. 2018, doi: 10.1063/1.5025025.
- [122] Z. Zhang *et al.*, “Kirigami-Inspired Stretchable Conjugated Electronics,” *Advanced Electronic Materials*, vol. 6, no. 1, p. 1900929, Jan. 2020, doi: 10.1002/aelm.201900929.
- [123] W. Zheng *et al.*, “Kirigami-Inspired Highly Stretchable Nanoscale Devices Using Multidimensional Deformation of Monolayer MoS<sub>2</sub>,” *Chemistry of Materials*, vol. 30, no. 17, pp. 6063–6070, Sep. 2018, doi: 10.1021/acs.chemmater.8b02464.
- [124] Y. Bao *et al.*, “Customized Kirigami Electrodes for Flexible and Deformable Lithium-Ion Batteries,” *ACS Applied Materials & Interfaces*, vol. 12, no. 1, pp. 780–788, Jan. 2020, doi: 10.1021/acsami.9b18232.
- [125] R. Sun *et al.*, “Kirigami stretchable strain sensors with enhanced piezoelectricity induced by topological electrodes,” *Applied Physics Letters*, vol. 112, no. 25, p. 251904, Jun. 2018, doi: 10.1063/1.5025025.

- [126] N. Hu *et al.*, “Stretchable Kirigami Polyvinylidene Difluoride Thin Films for Energy Harvesting: Design, Analysis, and Performance,” *Physical Review Applied*, vol. 9, no. 2, p. 021002, Feb. 2018, doi: 10.1103/PhysRevApplied.9.021002.
- [127] C. Wu, X. Wang, L. Lin, H. Guo, and Z. L. Wang, “Paper-Based Triboelectric Nanogenerators Made of Stretchable Interlocking Kirigami Patterns,” *ACS Nano*, vol. 10, no. 4, pp. 4652–4659, Apr. 2016, doi: 10.1021/acsnano.6b00949.
- [128] Z. Lv *et al.*, “Editable Supercapacitors with Customizable Stretchability Based on Mechanically Strengthened Ultralong MnO<sub>2</sub> Nanowire Composite,” *Advanced Materials*, vol. 30, no. 2, p. 1704531, Jan. 2018, doi: 10.1002/adma.201704531.
- [129] Y. Bao *et al.*, “Customized Kirigami Electrodes for Flexible and Deformable Lithium-Ion Batteries,” *ACS Applied Materials & Interfaces*, vol. 12, no. 1, pp. 780–788, Jan. 2020, doi: 10.1021/acsaami.9b18232.
- [130] Z. Song *et al.*, “Kirigami-based stretchable lithium-ion batteries,” *Scientific Reports*, vol. 5, no. 1, p. 10988, Sep. 2015, doi: 10.1038/srep10988.
- [131] “PDMS: a review.” <https://www.elflow.com/microfluidic-reviews/general-microfluidics/the-polydimethylsiloxane-pdms-and-microfluidics/> (accessed Dec. 25, 2021).
- [132] Y. Li, S. Zhang, X. Li, V. R. N. Unnava, and F. Cicoira, “Highly stretchable PEDOT:PSS organic electrochemical transistors achieved via polyethylene glycol addition,” *Flexible and Printed Electronics*, vol. 4, no. 4, p. 044004, Nov. 2019, doi: 10.1088/2058-8585/ab5202.
- [133] R. Luo, H. Li, B. Du, S. Zhou, and Y. Zhu, “A simple strategy for high stretchable, flexible and conductive polymer films based on PEDOT:PSS-PDMS blends,” *Organic Electronics*, vol. 76, p. 105451, Jan. 2020, doi: 10.1016/j.orgel.2019.105451.
- [134] <https://www.autodesk.ca/>, “AutoCAD.”
- [135] D. J. Stokes, *Principles and Practice of Variable Pressure / Environmental Scanning Electron Microscopy (VP-ESEM)*. John Wiley and Sons, 2008.



- [136] A. di Gianfrancesco, “Technologies for chemical analyses, microstructural and inspection investigations,” in *Materials for Ultra-Supercritical and Advanced Ultra-Supercritical Power Plants*, Elsevier, 2017, pp. 197–245. doi: 10.1016/B978-0-08-100552-1.00008-7.
- [137] A. Vaidya and K. Pathak, “Mechanical stability of dental materials,” in *Applications of nanocomposite materials in dentistry*, A. M. Asiri and A. Mohammad, Eds. Woodhead Publishing, 2018, pp. 285–305.
- [138] J. J. Licari and D. W. Swanson, *Adhesives technology for electronic applications: materials, processing, reliability*, Second. 2011.
- [139] D. S. R. Petroudy, “Physical and mechanical properties of natural fibers,” in *Advanced High Strength Natural Fibre Composites in Construction*, M. Fan and F. Feng, Eds. Woodhead publishing, 2017, pp. 59–83.
- [140] H. Ryeol Choi, K. Jung, J. Choon Koo, J. Nam, and Y. Lee, “MICRO-ANNELID-LIKE ROBOT ACTUATED BY ARTIFICIAL MUSCLES BASED ON DIELECTRIC ELASTOMERS,” in *Dielectric Elastomers as Electromechanical Transducers*, Elsevier, 2008, pp. 259–269. doi: 10.1016/B978-0-08-047488-5.00025-3.
- [141] X. Zhang, *Fundamentals of fiber science*. DEStech Publications, Inc, 2014.
- [142] J. W. S. Hearle and W. E. Morton, *Physical properties of textile fibres*, Fourth. Woodhead Publishing , 2008.
- [143] S. Kamrava, D. Mousanezhad, H. Ebrahimi, R. Ghosh, and A. Vaziri, “Origami-based cellular metamaterial with auxetic, bistable, and self-locking properties,” *Scientific Reports*, vol. 7, no. 1, p. 46046, Aug. 2017, doi: 10.1038/srep46046.
- [144] Y. Tang and J. Yin, “Design of cut unit geometry in hierarchical kirigami-based auxetic metamaterials for high stretchability and compressibility,” *Extreme Mech Lett*, vol. 12, Apr. 2017, doi: 10.1016/j.eml.2016.07.005.
- [145] D. M. J. Dykstra, J. Busink, B. Ennis, and C. Coulais, “Viscoelastic Snapping Metamaterials,” *Journal of Applied Mechanics*, vol. 86, no. 11, Nov. 2019, doi: 10.1115/1.4044036.

- [146] J. Diani, B. Fayolle, and P. Gilormini, “A review on the Mullins effect,” *European Polymer Journal*, vol. 45, no. 3, pp. 601–612, Mar. 2009, doi: 10.1016/j.eurpolymj.2008.11.017.
- [147] G. Ayoub, F. Zaïri, M. Naït-Abdelaziz, and J. M. Gloaguen, “Modeling the low-cycle fatigue behavior of visco-hyperelastic elastomeric materials using a new network alteration theory: Application to styrene-butadiene rubber,” *Journal of the Mechanics and Physics of Solids*, vol. 59, no. 2, pp. 473–495, Feb. 2011, doi: 10.1016/j.jmps.2010.09.016.
- [148] M. Makki *et al.*, “Mullins effect in polyethylene and its dependency on crystal content: A network alteration model,” *Journal of the Mechanical Behavior of Biomedical Materials*, vol. 75, pp. 442–454, Nov. 2017, doi: 10.1016/j.jmbbm.2017.04.022.
- [149] “<https://www.mathworks.com/products/matlab.html>.” <https://www.mathworks.com/products/matlab.html> (accessed Jan. 10, 2022).
- [150] “<https://www.mathworks.com/help/matlab/ref/trapz.html>.” <https://www.mathworks.com/help/matlab/ref/trapz.html> (accessed Jan. 10, 2022).
- [151] M. Gavazzoni, S. Foletti, and D. Pasini, “Cyclic response of 3D printed metamaterials with soft cellular architecture: The interplay between as-built defects, material and geometric non-linearity,” *Journal of the Mechanics and Physics of Solids*, vol. 158, p. 104688, Jan. 2022, doi: 10.1016/j.jmps.2021.104688.
- [152] A. D. Drozdov, “Cyclic viscoelastoplasticity and low-cycle fatigue of polymer composites,” *International Journal of Solids and Structures*, vol. 48, no. 13, pp. 2026–2040, Jun. 2011, doi: 10.1016/j.ijsolstr.2011.03.009.
- [153] D. D. L. Chung, “Polymer-Matrix Composites: Functional Properties,” in *Carbon Composites*, Elsevier, 2017, pp. 256–332. doi: 10.1016/B978-0-12-804459-9.00005-1.

- [154] A. Chhetry, Md. Sharifuzzaman, H. Yoon, S. Sharma, X. Xuan, and J. Y. Park, “MoS<sub>2</sub>-Decorated Laser-Induced Graphene for a Highly Sensitive, Hysteresis-free, and Reliable Piezoresistive Strain Sensor,” *ACS Applied Materials & Interfaces*, vol. 11, no. 25, pp. 22531–22542, Jun. 2019, doi: 10.1021/acsami.9b04915.

## APPENDIX A SUPPORTING INFORMATION

The linear current-voltage characteristics of the unstrained (in closed form) kirigami structured polymer composite suggest the Ohmic behavior as displayed in Figure A.1.

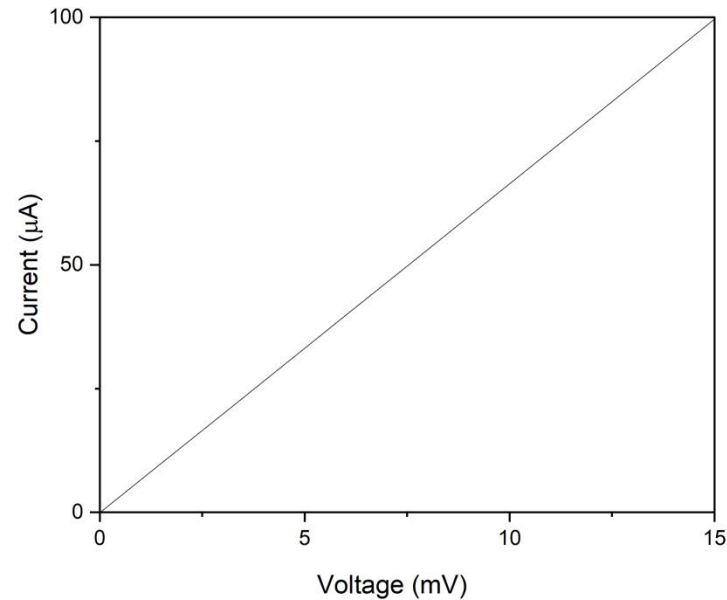


Figure A.1 The current-voltage curve of the kirigami sample in closed form (unstrained).

To calculate the area inside of each curve in Figures 1-4, the trapz [150] method of MATLAB [149] was used. The trapz method uses the trapezoidal technique to calculate the area under a curve or inside a closed curve. Following shows part of the code in MATLAB that we wrote to calculate the energy dissipation of samples one loading/unloading cycle at 25% strain:

```

A1=dlmread(file1);
figure(1);
x1=A1(:,1);
y1=A1(:,2);
a1 = trapz(x1,y1);
ha1=fill(x1,y1,'r');
xlabel('Displacement (mm)');
ylabel('Force (N)');
a1str = sprintf('Area = %6.4f', a1);
legend(ha1, a1str, 'Location','northwest');
grid off;

```

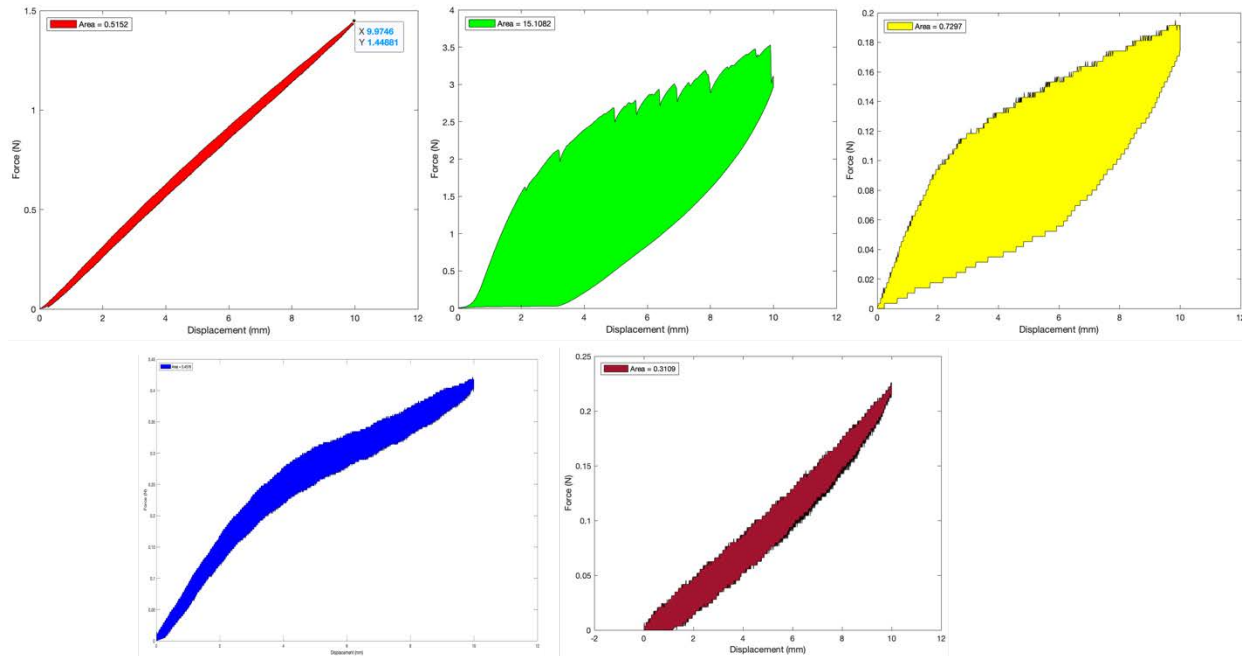


Figure A.2 Calculation of area between hysteresis loop using MATLAB software

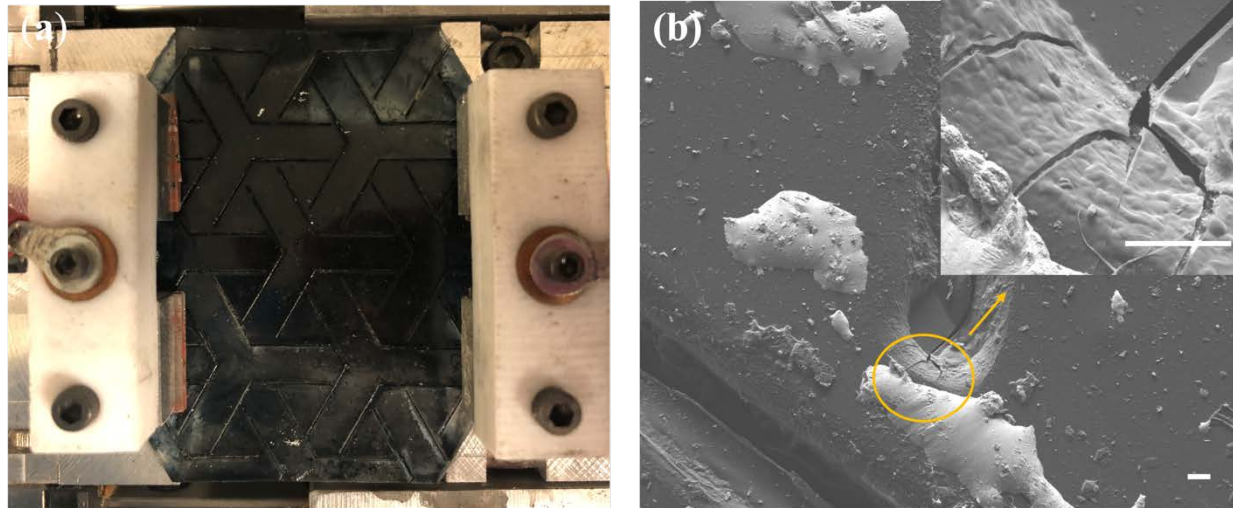


Figure A.3 (a) real image and (b) SEM images of kirigami structured PEDOT:PSS coated PDMS specimen after 5000 opening/closing in the closed-form. The scale bar is 100  $\mu\text{m}$ .